Tectonophysics 859 (2023) 229898

Contents lists available at ScienceDirect

Tectonophysics

journal homepage: www.elsevier.com/locate/tecto

Assessing the variability in hydraulic fracturing-induced seismicity occurrence between North American shale plays

James P. Verdon *, Germán Rodríguez-Pradilla

School of Earth Sciences, University of Bristol, Wills Memorial Building, Queen's Road, Bristol BS8 1RJ, UK

ARTICLE INFO

Keywords:
Induced seismicity
Hydraulic fracturing
Permeability
Shale gas
Tight gas

ABSTRACT

We examine differences in the occurrence rates of hydraulic fracturing-induced seismicity (HF-IS) between different shale plays in North America. While previous studies have investigated variations in HF-IS prevalence within individual plays, no studies have compared HF-IS occurrence between different plays. Our study examines associations between hydraulic fracturing and induced seismicity across 12 shale plays: the Barnett, Bakken, Duvernay, Eagle Ford, Fayetteville, Haynesville, Horn River, Marcellus, Montney, Niobrara, Utica, and Woodford. We compile earthquake catalogues for each play using a combination of data from published studies and regional and national earthquake databases. For plays in the United States we compile well data from the FracFocus database, while for Canadian plays we compile well data provided by provincial regulators. We use a rate-change approach to identify potential cases of HF-IS, where increases in earthquake rates above a background level in spatial and temporal proximity to active wells is taken to indicate a likelihood that seismic events are induced by hydraulic fracturing. We find very large variations, of several orders of magnitude, in the occurrence rates of HF-IS between different plays: for some plays we find an average rate of one $M \geq 2.0$ event per 3 wells, while some plays do not have any plausible cases of HF-IS despite hydraulic fracturing of many thousands of wells, and injection of several hundred million m^3 of fluid. We interpret these variations with respect to the underlying geological conditions. We find that geomechanical connections into basement rocks may promote HF-IS, but there are plays without such connections that have also generated significant levels of induced seismicity. We find that HF-IS is more prevalent in plays with high pore pressure gradients and strike-slip to compressive stress regimes. A multiple linear regression finds statistically significant fit between these two parameters in tandem and the observed rates of HF-IS occurrence.

1. Introduction

Hydraulic fracturing in shale plays has been demonstrated to have caused induced seismicity (e.g., Schultz et al., 2020; Verdon and Bommer, 2021a). However, the prevalence of hydraulic fracturing-induced seismicity (HF-IS) varies significantly, both within individual plays, and between different plays. The operational parameters for hydraulic fracturing in regions that are more and less prone to HF-IS are often very similar (with respect to, for example, injection volumes, rates, pressures, and injected fluid properties, e.g., McKeon, 2011). The similarities in operational parameters imply that the observed variability in HF-IS occurrence is driven by variations in geological conditions that promote or preclude induced seismicity. Hence, if we can quantify variations in HF-IS prevalence between different plays, and thereby identify the geological factors that influence the occurrence of HF-IS, then this information could be used to inform induced seismicity hazard assessment for future HF plays for which rates of HF-IS are not yet well-established (e.g., Verdon and Bommer, 2021a; Schultz et al., 2021).

The objective of this study is to quantify the relative prevalence of HF-IS in different shale plays. We focus on North America, as this continent has seen extensive use of hydraulic fracturing in a wide range of shale plays. Moreover, as regulators have recognised the significance of this issue, relevant data is becoming increasingly available, including data on injection wells via, for example, FracFocus (www.FracFocus.org) and earthquake data from dedicated regional monitoring networks (e.g., Fereidoni and Cui, 2015; Savvaidis et al., 2019; Walter et al., 2020). Having quantified the relative prevalence of HF-IS between different plays, we can then examine the extent to which different geological factors can account for the observed variabilities.

* Corresponding author.
E-mail address: James.Verdon@bristol.ac.uk (J.P. Verdon).

https://doi.org/10.1016/j.tecto.2023.229898
Received 14 February 2023; Received in revised form 20 April 2023; Accepted 4 May 2023
Available online 13 May 2023

1.1. Causative mechanisms for HF-IS

Before doing so, we begin by examining the factors that might be expected to account for the variabilities in HF-IS from a theoretical basis, and by reviewing previous studies that have sought to explain variations in HF-IS within individual shale plays.

Many studies of HF-IS have sought to understand the causative mechanisms that have generated HF-IS at individual sites (e.g., Schultz et al., 2015a; Deng et al., 2016; Clarke et al., 2019; Kettlety et al., 2020, 2021; Igonin et al., 2021, 2022; Cao et al., 2022). The fundamental geomechanical basis underpinning most such studies is that hydraulic fracturing creates perturbations in stress and pore pressure on pre-existing tectonic faults. The in-situ stresses acting on a pre-existing fault can be resolved into normal stress, σ_n, and shear stress, τ, components. A fault will slip if the stress conditions exceed the failure envelope given by:

$$\tau > \mu_f(\sigma_n - P_f) + C_h, \tag{1}$$

where P_f is the pore pressure, μ_f is the friction coefficient, and C_h is the cohesion of the fault. Hence, perturbations in stress and/or pore pressure that increase the Coulomb Failure Stress (CFS), given by:

$$CFS = \tau - \mu_f(\sigma_n - P_f) \tag{2}$$

will increase the likelihood of a fault slipping and generating induced seismicity.

Hydraulic fracturing involves the injection of fluids at high pressure. As shown by Eq. 2, increases in P_f will increase CFS, leading to fault slip. The migration of pressurised fluids into faults is typically invoked as the primary mechanism that generates induced seismicity (e.g., Schultz et al., 2015a; Igonin et al., 2021; Kettlety et al., 2021; Cao et al., 2022). In addition, the tensile opening of fractures during hydraulic fracturing creates geomechanical deformation in the surrounding rocks. Depending on their orientation and position relative to the hydraulic fractures, this poroelastic deformation can increase CFS on nearby faults. This mechanism has also been invoked as a causative mechanism for generating induced seismicity (e.g., Deng et al., 2016; Kettlety et al., 2020; Igonin et al., 2022).

From this understanding of the mechanisms that generate HF-IS, the necessary conditions are that:

1. Pre-existing faults are present.
2. The faults must be within sufficient proximity to the stimulated well such that either they are reached by the pressurised injected fluid, or they are perturbed by the poroelastic deformation generated by opening fractures.
3. The stress conditions on the faults (or a subset thereof) must be such that the CFS change required to reach failure (Eq. 1) is smaller than the perturbation generated by the hydraulic fracturing.

Hence, from a theoretical standpoint, the prevalence of HF-IS will be governed by three factors:

1. Abundance of faulting: a higher abundance of faulting will increase the likelihood that a given set of hydraulic fractures will intersect a pre-existing fault of sufficient size to generate felt seismicity.
2. Stress conditions: the stress conditions must be such that faults are near to the CFS threshold. Faults that are already in a condition close to the failure envelope given by Eq. 1 require only a small perturbation to induce slip. Such faults are referred to as being "critically stressed" (Zoback and Healy, 1992). Critically stressed faults are particularly prone to generating HF-IS (e.g., Kettlety et al., 2021). This condition will generally be favoured by high stress anisotropy (the difference between maximum and minimum principal stresses), and high pore pressure (which reduces the effective normal stress, $\sigma_n - P_f$). If faults have a preferred orientation, then induced seismicity will be favoured if the faults are well-oriented for slip in the in situ stress field.
3. Extent and magnitude of the hydraulic fracturing perturbation: the larger a volume of rock perturbed by a given stimulation, and the larger the magnitude of the perturbation, the greater the likelihood of intersecting a fault and exceeding its slip threshold. The size of the perturbation may be affected by operational factors (injection rate, cumulative volume, pressure and fluid properties) and the hydraulic properties of the formation (e.g., porosity, permeability, the presence of permeable fracture pathways). However, while the design of fracture stimulations does vary between different plays, there is typically considerable overlap with respect to operational factors such as injection volumes and rates, well lengths and stage spacings (e.g., McKeon, 2011).

1.2. Seismogenic index

The seismogenic index, S_I (Shapiro et al., 2010) relates the number of induced earthquakes, N_E, to the injected volume V, for a given minimum magnitude, M:

$$S_I = log\left(\frac{N_E}{V}\right) + bM, \tag{3}$$

where b is the Gutenberg and Richter (1944) b value. S_I is commonly used to quantify the rate of occurrence of induced seismicity during operations (e.g., Kwiatek et al., 2019; Kettlety et al., 2021), and can be used to forecast the largest magnitude event expected during operations, M_{MAX}:

$$M_{MAX} = \left(S_I - log\left[\frac{-ln\chi}{V_T}\right]\right) \Big/ b, \tag{4}$$

where V_T is the total planned injection volume, and χ is the probability that this magnitude is not exceeded.

While S_I is now most commonly used to quantify rates of induced seismicity and forecast M_{MAX}, its original formulation was based on a consideration of the geomechanical conditions within a given reservoir (e.g., Dinske and Shapiro, 2013), where the seismogenic index is given by:

$$S_I = log\left(\frac{10^a F}{C.S}\right), \tag{5}$$

where a is the Gutenberg-Richter a value, F is the density of faults around the injection point, C is the critical pore pressure increase required to reactivate the faults, and S is the storativity of the formation, which determines the magnitude and extent of the pressure increase created by the injection of a given volume. Hence, this formulation of S_I mirrors our understanding of the key factors that control the abundance of induced seismicity, as described in the previous section. Moreover, Eq. 5 describes how differences in stress conditions and/or faulting abundance between localities could be translated into different levels of induced seismicity hazard.

1.3. Variations of HF-IS within shale plays

Significant variations in HF-IS prevalence can occur within a shale play over a relatively short distance. As an example, in the Duvernay Formation in the Western Canada Sedimentary Basin (WCSB), HF-IS has predominantly occurred within two areas, Fox Creek (Schultz et al., 2015a) and Willisden Green (Schultz and Wang, 2020). Outside of these areas, the occurrence of HF-IS in the Duvernay has been limited or non-existent (Rodríguez-Pradilla et al., 2022). As shown in Fig. 1, within the Fox Creek area as the use of hydraulic fracturing has moved eastward by a few 10s of km, levels of HF-IS have decreased substantially (Reyes-

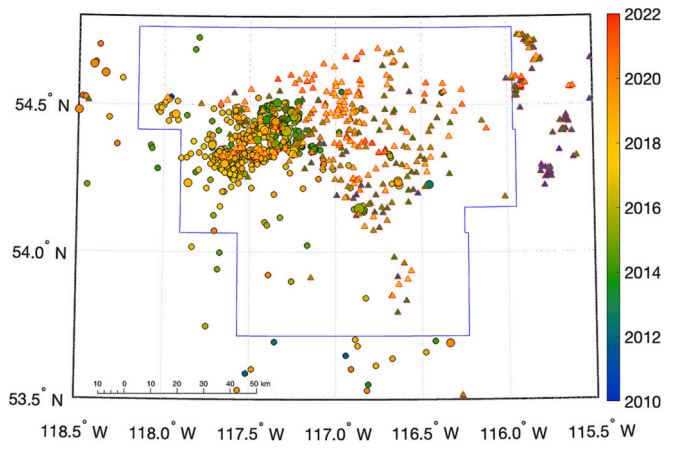

Fig. 1. Map of the Fox Creek region in the WCSB, showing hydraulic fracturing wells targeting the Duvernay Formation (red-outlined triangles) and earthquakes (black-outlined circles, sized by magnitude) since 2010. The blue line shows the area regulated by a Traffic Light Scheme as per the Alberta Energy Regulator Subsurface Order 2. Wells and earthquakes are coloured by year. (For interpretation of the references to colour in this figure legend, the reader is referred to the web version of this article.)

Canales et al., 2022).

Several studies have sought to examine the underlying causes of the observed variability in HF-IS occurrence within individual shale plays, including cases within the WCSB, Oklahoma, and Texas. Schultz et al. (2016) analysed the spatial distribution of HF-IS in the Duvernay Formation relative to the edges of the Swan Hills reefs. The Swan Hills Formation underlies the Duvernay, and the nucleation of reef formation in the WCSB Devonian section is thought to have been controlled by active tectonics at the time of deposition. As such, the edges of the Swan Hills reef formations are thought to denote the presence of dip-slip faulting in the underlying basement rocks. Schultz et al. (2016) found strong correlation between HF-IS and the edges of the Swan Hills reefs, with most cases being found within 20 km of reef edges. Hence, Schultz et al. (2016) describe a correlation between HF-IS and a proxy indicator of fault abundance.

Eaton and Schultz (2018) compared the occurrence of HF-IS in both the Duvernay and Montney Formations to the presence of overpressure in these shales. Pore pressure gradients (ΔP_f) in both formations are highly variable, ranging from near hydrostatic (10 kPa/m) to nearly 20 kPa/m. In both formations they found clear, statistically significant correlation between the occurrence of HF-IS and ΔP_f values higher than 15 kPa/m.

Pawley et al. (2018) used a logistic regression machine learning algorithm (LR-MLA) to examine how a range of geological factors contributes to induced seismicity in the Duvernay Formation. They studied a selection of model features including: depth to basement; ΔP_f; the minimum horizontal stress, S_{Hmin}; the natural seismicity rate; the thickness of the Duvernay Formation; the presence of dolomite within the Duvernay; the concentrations of lithium within pore fluids; the distance to mapped fault lineaments; and the distance to Devonian reef formations. Lithium concentration and the presence of dolomite were chosen as they might serve as proxies for hydraulic connectivity to the basement, since fluids circulating within the basement are Li-enriched and have been proposed as a driver for dolomitisation.

They found that the strongest control on HF-IS occurrence, as measured by their Information Gain Score, was proximity to basement, with ΔP_f, S_{Hmin}, distance to reef edges, and Li concentration also showing statistically significant information gain for HF-IS occurrence. Factors that did not appear to control HF-IS occurrence included the distance to mapped lineaments, the Duvernay Formation thickness, and the presence of dolomite.

Wozniakowska and Eaton (2020) used the same LR-MLA approach to investigate HF-IS in the Montney Formation. Their model inputs included distance from mapped faults, ΔP_f; proximity to basement; proximity to the Debolt Formation; injection depth; distance to the Cordilleran deformation front; depth level within the Montney Formation; and the difference between the local and the regional-average S_{HMAX} orientation. The Debolt Formation is a massive carbonate formation of Carboniferous age, which underlines the Montney. The Debolt has been shown to have significant mechanical strength which could enable it to host larger seismic events. The Cordilleran deformation front delineates the zone of extensive fold-and-thrust deformation generated by the growth of the Rocky Mountains during the Laramide Orogeny. The difference between local and regional S_{HMAX} orientation was used as a potential proxy for the presence of critically stressed faults, as active faults can produce local rotation of the stress field.

They found that the most significant control on HF-IS occurrence was the distance to the Cordilleran deformation front. Other significant factors included the injection depth, the distance to basement, ΔP_f, and the local S_{HMAX} variance. Factors that were not significant were the distance to the Debolt Formation, the depth level within the Montney, and the distance to mapped faults.

Fox et al. (2020) used multivariate statistical analysis to examine Montney HF-IS. Their model inputs comprised over 50 parameters, including both geological and operational factors. Geological factors included distances from mapped faults, ΔP_f and ΔS_{HMAX}, target depth, and the curvature of selected subsurface horizons (which can be used as a proxy for faulting). Operational factors included fluid volumes, breakdown pressures, evidence for screen-outs, well length, and breakdown and shut-in pressures. They computed two models, firstly classifying for the occurrence or absence of HF-IS, and then a regression to induced seismicity magnitudes. Given the number of model parameters, the results of Fox et al. (2020) can't be easily summarised. However, they consistently found that geological factors were more important than operational factors in explaining the variations in induced seismicity across the play. Geological factors of particular note included injection depth, distance from mapped faults, pore pressure and minimum horizontal stress parameters, and the curvature of relevant geological horizons.

Fasola et al. (2019) studied HF-IS in the Eagle Ford Shale of southern Texas, searching for qualitative correlations between the percentages of wells experiencing HF-IS and the local geological conditions. They found an increase in HF-IS prevalence in proximity to the Karnes Trough southern bounding fault, and an increase in HF-IS where the Austin Chalk Formation was present. They also examined the prevalence of HF-IS with respect to operational factors, finding an increased likelihood of seismicity when multiple wells were stimulated simultaneously from the same pad, which was attributed to an overall larger injection volume within a comparable area.

The majority of the induced seismicity observed in Oklahoma has been driven by WWD into the Arbuckle Formation (e.g., Keranen et al., 2013). However, Skoumal et al. (2018) identified a significant number of cases where seismicity has been generated by hydraulic fracturing, primarily within the Woodford Shale. Ries et al. (2020) examined these HF-IS cases with respect to both operational and geological factors, using a logistic regression method. Operational factors examined included the use of multi-well pads, injection volumes, and the use of slickwater versus gel. Geological factors included the well depth, the proximity to the crystalline basement, and the geological age of the formation being targeted (evidently there will be significant co-dependence between these parameters).

They found that there was no correlation between injection volumes and HF-IS prevalence, but they did find a significant correlation between HF-IS and the use of slickwater versus gelled frac fluids. However, the choice of fluid is likely to be formation-dependent, with gelled fluids more likely to be used in shallower tight gas sandstone formations, and slickwater more commonly used in deeper shale formations. They found

the wells targeting deeper and older formations were more likely to generate HF-IS, but once this trend is accounted for, they did not observe any trend between proximity to basement and HF-IS. Ries et al. (2020) interpreted the increased HF-IS prevalence with depth as being driven by increased overpressure with depth within the basin.

McKeighan et al. (2022) compared the occurrence of HF-IS in the Eagle Ford play with detailed fault maps in the region. They found that 70% of "seismogenic faults" identified from lineations of earthquake hypocentres were located within 1 km of a known, mapped fault. They examined the stress conditions on these faults, finding that induced seismicity occurred on faults with a range of stability conditions, including those which would have required significant perturbation (> 8 MPa) to reactivate. However, we note that the areas with the highest levels of HF-IS (the KTFZ-SW, KTFZ-central, and KTFZ-NE areas, as defined by McKeighan et al., 2022) had large numbers of faults with low stability conditions (perturbations required for failure of <2 MPa).

We summarise our theoretical considerations and the observations of HF-IS variability within shale plays as follows. Our theoretical considerations suggest that the key geological controls on HF-IS prevalence will be fault abundance and effective stress conditions. Observational studies of HF-IS variability within plays have generally reached similar conclusions, finding that HF-IS occurs preferentially in areas with higher pore pressure gradients and lower S_{Hmin} (and hence higher shear stresses). These studies have also found HF-IS to be correlated with various different factors that are assumed as proxies for the abundance of faulting (e.g., formation depth, distance to basement, lithium concentrations, distance to Cordilleran fronts, etc.).

2. Assessment of HF-IS variability

Fig. 2 shows major shale plays in North America in which hydraulic fracturing has been used extensively. Fig. 3 shows the total number of hydraulically fractured wells per year and the total fluid volumes injected for hydraulic fracturing in each of the labelled plays. The decrease in well numbers and fluid volumes in 2015–16 was driven by the collapse in hydrocarbon prices at this time (Stocker et al., 2018), while the decrease in activity in 2020 was driven by the drop in prices during the COVID-19 pandemic.

The injection data for WCSB plays is taken from hydraulic fracturing databases published by the Alberta Energy Regulator and by the British Colombia Oil and Gas Commission. These combined datasets include over 36,000 hydraulically fractured wells. Given the regulatory environment in these provinces, we believe that this database is relatively complete for the periods under consideration in our study.

The injection data for plays in the USA is taken from the FracFocus database (Dundon et al., 2015), which was launched in 2011. The FracFocus database contains records from over 195,000 hydraulically fractured wells in the USA. However, regulations pertaining submission of data to FracFocus have varied by jurisdiction. Hence, it is difficult to assess the completeness of the database. However, this remains the only nationwide database of hydraulic fracturing wells that is conveniently available for the USA. For all injection datasets, we have well locations, start and end dates for operations, and total injected volumes. The earthquake catalogues we use for each shale play are described in the Appendix.

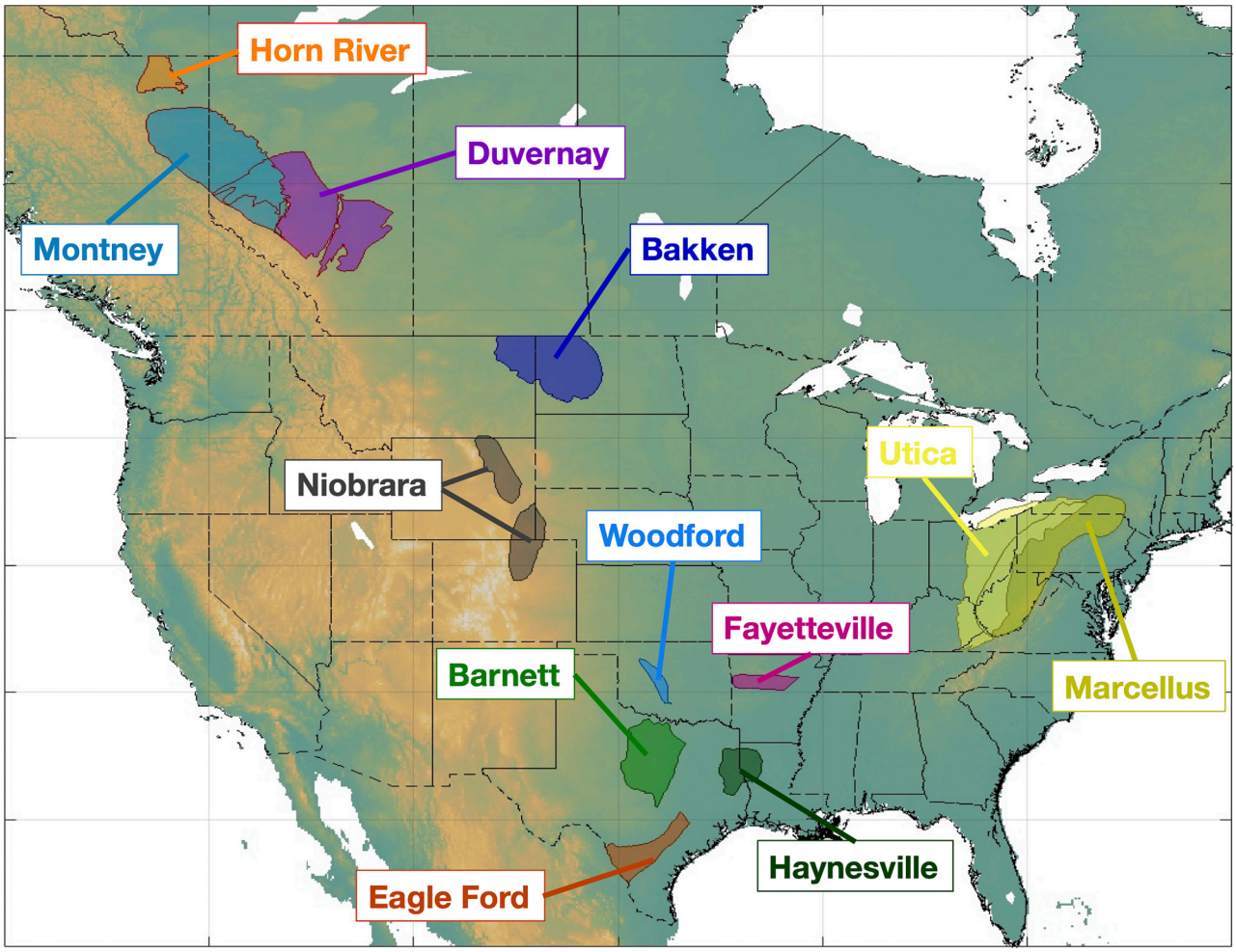

Fig. 2. Map showing major North American unconventional plays.

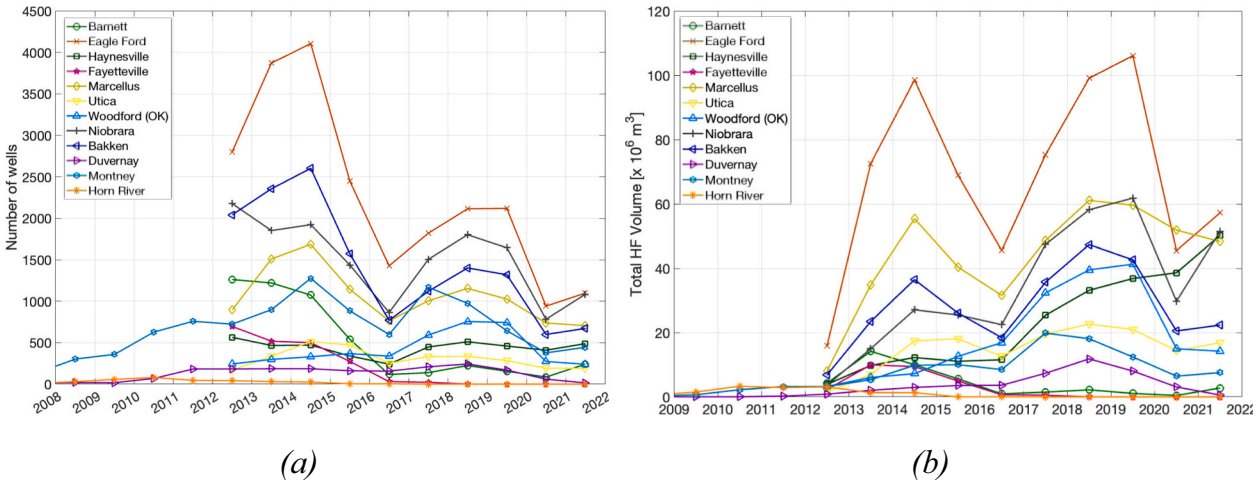

Fig. 3. Activity rates in major North American shale plays. In (a) we show the numbers of wells completed per year, and in (b) we show the total annual fluid volumes used for HF in each play.

The major challenge in assessing HF-IS prevalence is in identifying which earthquakes within a basin have been caused by hydraulic fracturing. In addition to HF-IS events, seismicity may occur naturally, and earthquakes may also be induced by other co-located activities such as conventional hydrocarbon production (e.g., Segall, 1989), fluid injection for enhanced oil recovery (EOR, e.g., Gan and Frohlich, 2012), or wastewater disposal (WWD, e.g., Healy et al., 1968). Discriminating between induced earthquakes and natural events, and indeed discriminating between HF-IS and seismicity caused by other industrial activities such as WWD, is challenging, and detailed examination of the spatial and temporal evolution of seismicity relative to various industrial activities may be required to definitively establish causation (e.g., Verdon et al., 2019).

Some studies (e.g., Ghofrani and Atkinson, 2020) have used simple spatio-temporal filters to assign causation (any event within a given time and distance of a hydraulic fracturing operation is assumed to be a potential case of HF-IS). However, it has been shown that this approach frequently mischaracterises the causes of seismicity, especially when multiple industrial activities such as WWD and hydraulic fracturing are co-located (Verdon and Bommer, 2021b). Grigoratos et al. (2020) developed a method to assess causative factors for induced seismicity based on statistical correlations between industrial activities and earthquake rates within discretised area blocks. Skoumal et al. (2018) assessed causation using a seismicity rate-change method, whereby HF-IS was identified for cases where the rate of seismicity during a hydraulic fracturing operation (within a given distance) was significantly higher than the rate of seismicity within a period before and after the operation. Skoumal et al. (2018) used a distance of 10 km from an operation, time periods either side of an operation of 5 to 30 days, and required the earthquake rate during operations to be at least 10 times larger than the baseline rate.

We adopt a similar approach to Skoumal et al. (2018) in our analysis, recognising its ease of application in comparison to the Grigoratos et al. (2020) method, yet with an ability to discriminate HF-IS with WWD-IS since we might expect WWD to produce seismicity rates that are elevated within a particular area over an extended period of time.

We use 10 km as our distance criterion. Where detailed microseismic observations have been made (e.g., Igonin et al., 2021; Kettlety et al., 2021), induced seismicity is generally observed to occur within 1, or at most 2 km from the causative well. However, incorporating larger distances into our analysis allows for the presence of horizontal wells, which will increase the potential distance from the wellhead to the induced seismicity, and allows for uncertain event locations produced by regional monitoring networks, which can often be of several km (e.g., Schultz et al., 2015b).

For each well, we compute the number of $M \geq 2.0$ events within 10 km of the well that occur during the "well active" period, defined as running from the start of operations until 10 days after the end of operations. We extend the active period after the end of injection to incorporate the possibility of trailing events, which typically occur within this timeframe (e.g., Verdon and Bommer, 2021a).

We compare the rate of seismicity during the active period to the background rate of seismicity within the same area within a period extending 6 months (182 days) before the start of operations, and 6 months after the end of the active period. We choose a longer period over which to compute the baseline in comparison to Skoumal et al. (2018) in recognition of the fact that WWD typically produces sequences of seismicity that extend over multi-year timescales (e.g., Watkins et al., 2023), and so a longer baseline period may be more appropriate. Our change in earthquake rate is then given by:

$$\Delta R = \frac{R_{active}}{R_{baseline}}, \tag{6}$$

where R_{active} and $R_{baseline}$ are the rates (average number of events per day) during the active and baseline periods, respectively. Where no events are observed during the baseline period, we adopt a value for $R_{baseline}$ of 1/365: i.e., allowing for the possibility of 1 earthquake occurring within the baseline period. We use $\Delta R \geq 5$ as our threshold to indicate a potential case of HF-IS. This is slightly more lenient than the threshold used by Skoumal et al. (2018), which reflects our objective to capture more potential cases of HF-IS, while accepting that more cases identified as HF-IS might represent false positives.

In adopting this approach, we accept that some cases of HF-IS may be missed by our analysis, and that some cases identified as HF-IS may be spurious, either being caused by other industrial activities, or being natural earthquakes. Hence, any individual case identified here should not be considered as definitively demonstrated to be (or not to be) a case of HF-IS. However, our primary objective in this study is to produce a relative comparison of HF-IS abundance between shale plays across North America. Hence, since we apply the same method to each play, any misidentifications of causation should be evened out at relatively similar rates across each play. Moreover, as shown in our Results, the observed prevalence of HF-IS varies by many orders of magnitude between different plays, so the occasional reassessment of causation to remove some false positives, or to include some false negatives, would not have a major impact in our overall ranking of plays with respect to the prevalence of HF-IS.

3. Results

Table 1 lists the numbers of HF-IS events identified for each play. More detailed descriptions of events identified within each play are provided within the Appendix. To normalise the observed numbers of events we compare the numbers of events versus the total number of wells N_E/N_W. This parameter does not represent the number of wells with associated events, since some wells may have more than one associated event, and in some cases an event may have a potential association with more than one well. Hence, we also present the number of wells that have potential associated events, and with N_{WA}/N_W we express this as a fraction of the total number of wells.

Since the average volumes injected by each well in different plays may vary, we also compute S_I as defined in Eq. 3, and the seismic efficiency, S_{EFF} (Hallo et al., 2014), which is given by:

$$S_{EFF} = \frac{\Sigma M_o}{G\Delta V}, \tag{7}$$

where ΣM_O is the cumulative moment released by HF-IS events, G is the shear modulus (assumed to be 20 GPa as a generic value throughout this study), and ΔV is the total volume of injected fluid. In computing S_I, we use a default value of $b = 1.0$.

We observe very significant variations in HF-IS prevalence, with N_E/N_W, S_{EFF} and S_I ranging over at least 3.5 orders of magnitude. Some plays, such as the Barnett, Bakken and Niobrara, have experienced no cases of HF-IS (the handful of cases identified in Table 1 for these plays are likely to be false positives, see Appendix), whereas the Duvernay Formation, which has the highest prevalence of HF-IS, has experienced an average rate of 1 M ≥ 2.0 event per 3 wells, with roughly 1 in 10 wells being potentially associated with M ≥ 2.0 seismicity.

4. Discussion

4.1. Geological factors affecting HF-IS variation

Having classified the relative prevalence of HF-IS in different shale plays, we can begin to examine different geological factors that may have promoted (or inhibited) the occurrence of induced seismicity. We note that this is not a trivial exercise. Much of the relevant data is not publicly available. Where possible, we have sought to compile relevant information from the available literature. Many of the factors we aim to study will vary within each play, such that assigning a "typical" value is difficult. Likewise, as shown in Fig. 1 the prevalence of HF-IS is seldom uniform across a play, but tends to cluster in specific areas. As such, it can be challenging firstly to establish whether sparse data drawn from limited publicly available literature is representative of a play as a whole, and secondly whether the data is representative of the areas of a play that have experienced HF-IS. The geological factors that we have examined are summarised in Table 2 and discussed below and in the Appendix.

4.2. Involvement of basement rocks

In general, we expect that the stresses within the stiffer underlying basement rocks will be higher. As these rocks are also older, we would also expect them to have a greater abundance of faulting. These factors may make basement rocks more prone to generating more and larger induced seismic events. The transfer of pore pressures into basement rocks has often been invoked as a key factor for triggering WWD-induced seismicity in North America (e.g., Hincks et al., 2018). We therefore examine whether hydraulic or geomechanical connections into basement rocks have been a factor for HF-IS. Our assessment is summarised in Table 2, and further explanations for each play are provided in the Appendix.

We observe that plays which have low prevalence of HF-IS generally have clear hydraulic isolation from basement rocks. Many of the plays with high levels of HF-IS do show evidence for connections with basement rocks (e.g., the Duvernay, Horn River). However, some of the plays with high prevalence of HF-IS do not have basement involvement (e.g., the Montney and Fayetteville). Hence, we conclude that hydraulic or geomechanical connections into basement rocks can increase the likelihood of HF-IS. However, such connections are clearly not a necessary condition, as some plays without connections to basement rocks have also generated high levels of HF-IS.

Table 2
Geological factors for different plays.

Play	Basement involved	ΔP_f [kPa/m]	A_φ
Bakken	No	13.5–17	1.20 (E/SS)
Barnett	No	10–11.5	0.97 (E/SS)
Duvernay	Yes	> 15	1.71 (SS)
Eagle Ford	No	11–18	0.75 (E)
Fayetteville	No	19	1.57 (SS)
Haynesville	Uncertain	15–21	0.99 (E/SS)
Horn River	Yes	13–18	1.75 (SS)
Marcellus	No	9–15	1.95 (SS/C)
Montney	No	> 15	1.93 (SS/C)
Niobrara	No	12.6	0.90 (E/SS)
Utica	Yes	14–19	1.80 (SS/C)
Woodford	No	11–20	1.54 (SS)

Table 1
Rates of HF-IS identified in each major North American shale play.

Play	No. of Wells[1]	Total HF Volume [x10^6 m^3]	No. of Associated EQs[2]	Largest event magnitude[3]	$\log_{10}(S_{EFF})$	S_I	$\log_{10}(N_E/N_W)$	No. of Associated Wells	$\log_{10}(N_{WA}/N_W)$
Bakken	15,375	288	1	3.3	−4.72	−6.46	−4.19	3	−3.71
Barnett	6427	45	2	2.9	−4.49	−5.35	−3.51	3	−3.33
Duvernay	1946	44	569	4.1	−1.98	−2.89	−0.53	145	−1.13
Eagle Ford	15,825	407	389	3.7	−3.45	−4.19	−1.61	731	−1.34
Fayetteville	2863	28	421	3.9	−2.02	−2.82	−0.83	336	−0.93
Haynesville	3650	208	18	3.8	−5.38	−5.06	−2.31	9	−2.61
Horn River	344	14	30	3.6	−2.24	−3.67	−1.06	25	−1.14
Marcellus	11,530	456	2	2.8	−5.43	−6.36	−3.76	2	−3.76
Montney	8281	80	388	4.4	−2.00	−3.31	−1.33	603	−1.13
Niobrara	17,314	367	9	2.6	−5.34	−5.61	−3.28	45	−2.58
Utica	3146	157	37	3.8	−3.57	−4.63	−1.93	24	−2.12
Woodford	4424	198	794	3.6	−2.70	−3.40	−0.75	584	−0.88

[1] The number of wells and the total injected volume are for those wells included within our study period for each play. It may not be the total number of wells stimulated or the total injected volume during the entire life of any given play.
[2] In cases with small numbers of associated events, these associations are likely to represent coincidental association between earthquakes and wells, and should not be taken to imply evidence for causation.
[3] As above, where associations are likely spurious, the largest "associated" event may not have been caused by hydraulic fracturing.

4.3. Stress field classification

Verdon and Bommer (2021a) proposed that the prevalence of HF-IS might be affected by the stress field classification within different plays. The crust is typically assumed to be near to critical stress conditions (Zoback et al., 2002). This assumption is especially true for sites that could be prone to HF-IS. As a result, stress conditions will be controlled by the frictional properties of faults, as shown in Fig. 4. The vertical stress, S_V, will always be determined by the overburden weight, which is primarily a function of depth. In an extensional stress regime, the horizontal stresses, S_{HMAX} and S_{Hmin}, must be less than S_V. Given the positive slope of the Mohr-Coulomb failure envelope, the resulting shear stresses must therefore be relatively small. This can be contrasted with a compressional stress regime, where both S_{HMAX} and S_{Hmin} will be larger than S_V, and so the shear stresses at criticality will be significantly larger. A strike-slip stress regime will be intermediate between these conditions in terms of shear stress magnitudes at criticality.

We might expect HF-IS to be favoured at sites with higher shear stresses. Hence, Verdon and Bommer (2021a) argued that HF-IS might be more prevalent in compressional faulting regimes, becoming less common through strike-slip and then extensional faulting regimes. We quantify the stress field classification using the A_φ parameter (Simpson, 1997), as mapped by across North America by Lund Snee and Zoback (2020). The stress field classification A_φ differentiates between extensional, strike-slip and compressional faulting regimes, where $0 < A_\varphi < 1$ implies an extensional regime, $1 < A_\varphi < 2$ implies a strike slip regime, and $2 < A_\varphi < 3$ implies a compressional regime. In Table 2 we show the average A_φ value within the boundaries of each play, along with a qualitative summary as defined below:

- $A_\varphi < 0.75$: extensional (E)
- $0.75 < A_\varphi < 1.25$: extensional to strike slip (E/SS)
- $1.25 < A_\varphi < 1.75$: strike slip (SS)
- $1.75 < A_\varphi < 2.25$: strike slip to compressional (SS/C)
- $A_\varphi > 2.25$: compressional (C).

We observe that there is some correlation between stress classification and HF-IS prevalence, albeit with significant outliers as well (Fig. 5a,b). Four of the five plays with low HF-IS prevalence are in extensional stress regimes ($A_\varphi \approx 1$). The only case that is not is the Marcellus, which has a strike-slip to compressional stress regime. Four of the five cases with high HF-IS prevalence are in strike-slip to compressional faulting regimes ($A_\varphi > 1.5$), the only exception being the Eagle Ford, which is in an extensional stress regime.

We surmise that the stress field classification (extensional, strike-slip or compressional) does play a role in determining the prevalence of HF-IS, but clearly this factor cannot be treated as definitive, as high levels of HF-IS have been generated in extensional regimes (e.g., the Eagle Ford), and low levels of HF-IS have been generated in compressional regimes (e.g., the Marcellus).

4.4. Pore pressure gradients

High pore pressures increase CFS by reducing the effective normal stresses that act to clamp faults, bringing faults towards failure. Hence, we might expect HF-IS to be more common in formations that have high in situ pore pressures. We note that high pore pressures are typically considered a good indicator of hydrocarbon production potential, so there is a potential trade-off between more effective production but increased HF-IS prevalence.

Since pore pressure values are primarily controlled by depth, variations in pore pressure are typically quantified in terms of pore pressure gradients, ΔP_f. A pore pressure gradient of 10 kPa/m denotes a hydrostatic pressure system, while larger values indicate overpressuring produced by the generation of hydrocarbons in the subsurface. Our literature sources for pore pressure gradients for each play are described in the Appendix. Where a range of pore pressure gradients are reported, we adopt values at the upper ends of these ranges, since we surmise that induced seismicity will be more prevalent in the areas of a given play that have higher pore pressure gradients (e.g., Eaton and Schultz, 2018).

We find positive correlation between pore pressure gradients and the prevalence of induced seismicity (Fig. 5c,d): all the cases with high induced seismicity prevalence have pore pressure gradients that exceed 15 kPa/m. However, we again note that elevated pore pressures do not guarantee that induced seismicity will occur – for example the Haynesville has extremely high pore pressure gradients and yet minimal occurrence of HF-IS.

4.5. Covariance of parameters

Given the correlations seen in Fig. 5, it is of interest to examine the variations in S_{EFF} and S_I as a function of both A_φ and ΔP_f. We therefore compute a multiple linear regression for S_{EFF} and S_I using both parameters. The resulting surfaces are shown in Fig. 6, and clearly show how high S_{EFF} and S_I values are expected when both A_φ and ΔP_f are high. The R^2 statistic for the S_{EFF} surface is 0.63 and the R^2 for the S_I surface is 0.65, reflecting the quality of the fitted surface to the observations. These values are significant at $P < 0.05$ ($P = 0.039$ and $P = 0.032$ respectively).

Given the number of different factors that could affect the prevalence of HF-IS, and the broad-brush approach that we have adopted, it is perhaps surprising that only two parameters can produce such an effective fit to the observed data. However, our results clearly show that elevated levels of HF-IS should be expected in plays with high pore pressure gradients and stress regimes with $A_\varphi > 1.5$.

4.6. Other geological factors

In addition to the parameters examined above, we would ideally

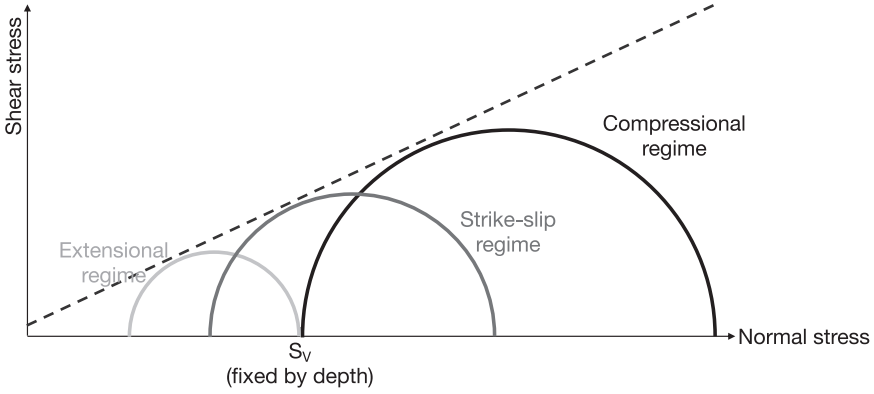

Fig. 4. Schematic depiction of the impact of stress regime (extensional, light grey; strike-slip, dark grey; compressional, black) on the shear stress that might be experienced by faults. We show Mohr circles for each stress condition, on the condition that the vertical stress, S_V, is fixed by depth, and that stress conditions are close to the Mohr-Coulomb failure criteria (dashed line). As such, the extensional regime produces lower shear stresses, while the compressional regime produces higher shear stresses. Adapted from Verdon and Bommer (2021a).

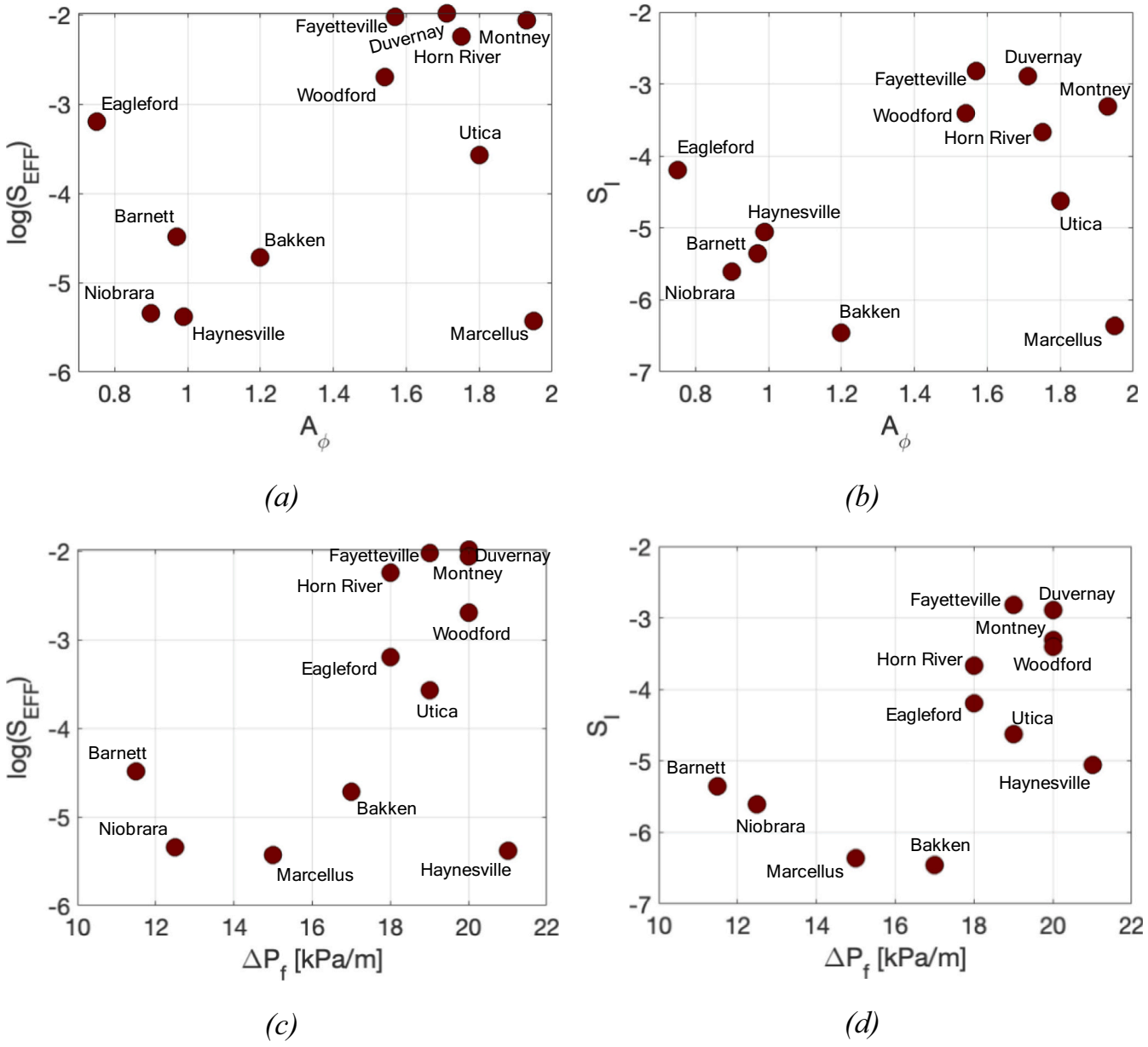

Fig. 5. Cross-plots of S_{EFF} (a,c) and S_I (b,d) as a function of A_φ (a,b) and ΔP_f (c,d) for each play described in Table 2. We generally see positive correlation between induced seismicity rates (S_{EFF} and S_I) and both A_φ and ΔP_f.

have liked to assess the role of stress gradients (in particular maximum and minimum stress gradients, and the differences between these gradients), and the abundance of faulting. However, we were not able to obtain any publicly available data on stress gradients for many of the plays. We were able to obtain fault map data for most of the plays. However, the resolution of these maps varied substantially. Some fault maps were derived from surface geological mapping, in which case the fault abundance will primarily be determined by the scale and resolution of the mapping and the availability of geological exposure. Others were derived from reflection seismic data, in which case the fault abundance is significantly higher than values obtained by geological mapping, but will primarily be determined by the availability and resolution of seismic data, which varies substantially across and between plays. We note that studies of HF-IS within individual plays have consistently found that proximity to abundant faulting (or various proxies thereof) correlates with HF-IS prevalence, as described above.

We also did not examine the role of permeability in promoting HF-IS. All of the plays we studied were shale plays, with permeabilities typically falling in the range 1×10^{-7} to 1×10^{-4} mD. Hydraulic fracturing has also been used for many decades in tight sandstone plays, without generating any published cases of HF-IS. For example, in the WCSB the focus of the research community with respect to HF-IS has been the Duvernay and Montney shales, but more wells have been hydraulically fractured in the shallower, Cretaceous-age Cardium and Mannville formations without generating any HF-IS (Verdon and Bommer, 2021b). These formations have permeabilities of the order 0.1 mD, and so are characterised as tight sandstone plays. Likewise, in the UK, hydraulic fracturing of the lower Carboniferous Bowland Shale has generated notable cases of HF-IS (Clarke et al., 2014, 2019; Kettlety et al., 2021), but hydraulic fracturing of the overlying Millstone Grits (a tight sandstone formation) has not generated any recorded cases (Mustanen et al., 2017). In 2013, an extensive study by the US National Research Council (NRC, 2013) concluded that hydraulic fracturing posed a low risk of induced seismicity. It is likely that they reached these conclusions because, at the time of their study, the majority of hydraulic fracturing data came from tight gas fields, which have not generated any

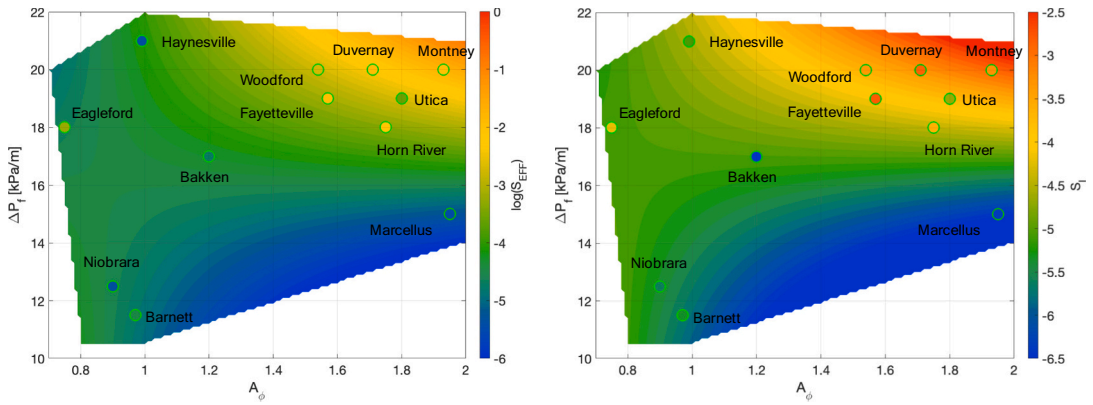

Fig. 6. Multiple linear regression for S_{EFF} (a) and S_I (b) as a function of A_φ and ΔP_f: the dots show our observations, and the contours show the best-fit surfaces.

identified cases of HF-IS.

One control that permeability may have on the generation of HF-IS is that in higher permeability formations, elevated pressures may be able to quickly disperse into the formation, minimising the magnitude and duration of the resulting perturbations. In contrast, in lower permeability formations, if fractures intersect a fault then elevated pressures may be directly transferred into the fault without any dissipation. This effect may be particularly pronounced if a formation contains high permeability fracture corridors within an otherwise low permeability rock, thereby permitting the fractures to serve as a conduit, delivering elevated pressures to faults at greater distances from the well (e.g., Galloway et al., 2018; Igonin et al., 2021). This effect would be significantly reduced if the rock matrix had a higher permeability. Clearly, further study to understand the differences in HF-IS prevalence between tight gas and shale formations is warranted.

5. Conclusions

We have examined the variability in occurrence of HF-IS between major shale plays in North America. We find very significant differences in occurrence rates, which vary by >3 orders of magnitude. The Duvernay Formation in the WCSB had the highest occurrence rates, with an average rate of occurrence of 1 $M \geq 2.0$ event per 3 wells, and 1 in 10 wells being potentially associated with HF-IS. The Woodford, Fayetteville, Eagle Ford, Montney, and Horn River plays also had notably elevated rates of HF-IS occurrence. In contrast, the Bakken, Barnett and Niobrara have likely not experienced any HF-IS (the few potential cases identified here are likely to be false positives), while the Marcellus and Haynesville have only experienced one and two documented cases, respectively.

We have examined three potential geological factors that might account for this variability: connections to basement rocks, pore pressure gradients, and stress field classification. In general, increased induced seismicity prevalence was associated with the presence of connections to basement rocks, higher pore pressure gradients, and strike-slip to compressive stress fields. However, no single factor was found to be necessary or definitive: we do see elevated rates of HF-IS in plays without basement connections (e.g., the Montney), and in plays in extensional settings (e.g., the Eagle Ford). All the plays with elevated rates of HF-IS had high pore pressure gradients, but some plays with high pore pressure gradients did not have elevated rates of HF-IS (e.g., the Haynesville). Multiple linear regression between HF-IS rates and a combination of pore pressure gradients and stress field classifications produced a statistically significant correlation, with play-wide S_{EFF} and S_I values being associated with a combination of high pore pressure gradients and high A_φ values.

Other factors such as faulting abundance and stress gradients could also influence HF-IS abundance, but we were not able to examine these factors because of a lack of available data. Likewise, the apparent lack of HF-IS associated with a long history of hydraulic fracturing in tight gas plays merits further investigation.

Author credit statement

Both authors contributed equally to this study. GRP compiled the datasets used in our analysis. JPV performed the analyses. JPV led the writing of the paper, with contributions and edits from GRP.

CRediT authorship contribution statement

James P. Verdon: Conceptualization, Data curation, Formal analysis, Funding acquisition, Investigation, Methodology, Project administration, Visualization, Writing – original draft, Writing – review & editing. **Germán Rodríguez-Pradilla:** Data curation, Investigation, Writing – review & editing.

Declaration of Competing Interest

The BUMPS project is funded by a range of operating and oilfield service companies, some of whom hold interests in the development of shale gas resources. In addition, JPV has acted as an independent consultant for a variety of organisations including hydrocarbon operating companies and governmental organisations on issues pertaining to induced seismicity. None of these organisations had any input into the conception, development, analysis or conclusions of this study.

Data availability

Earthquake catalogues used in this study were compiled from a range of regional and national earthquake catalogues, as well as from supplementary materials in published papers. In our Appendix we describe in detail the resources from which the catalogues for each shale play were compiled. The well data for the USA was compiled from FracFocus (www.fracfocus.org). The well data for the WCSB was compiled from PetroNinja (https://petroninja.com). The stress field classification data was taken from the supplementary materials of Lund Snee and Zoback (2020).

Acknowledgements

James Verdon and Germán Rodríguez-Pradilla's contributions to this study were funded by the Natural Environment Research Council

(NERC) under the SeisGreen Project (Grant No. NE/W009293/1), and by the Bristol University Microseismicity Project (BUMPS).

Appendix A. Categorisation of HF-IS prevalence in North American unconventional plays

A.1. Barnett Shale

The Barnett Shale in the Fort Worth Basin, northeastern Texas, was the first in which massive slickwater hydraulic fracturing was developed to produce shale gas. As such, it can be regarded as a prototype for shale gas development, and was the largest gas producer in the early 2000s, although it has now been superseded by other plays. >16,000 HF wells have been completed in this formation. Despite the extensive use of hydraulic fracturing, there have been no reported or published cases of HF-IS in the Barnett Shale. However, WWD in the underlying Ellenburger Formation has caused induced seismicity in this region (Frohlich, 2012).

A.1.1. Barnett Shale induced seismicity assessment

We compiled a composite earthquake catalogue for the Barnett play by combining the North Texas Earthquake Study catalogue (NTXES, Quinones et al., 2019), which runs from 2008 to 2018, with the Texas Seismological Network catalogue (TexNet, Savvaidis et al., 2019), which runs from 2017 to the present. Well data in the FracFocus database also runs from 2008 to the present. However, based on cumulative injection volumes within the dataset, which are below 1 million m^3 per year prior to 2012, we believe the dataset is missing large numbers of wells before this date. As such, our analysis is based solely on wells from 2012 onwards. Although this time window misses the main phase of development in the Barnett, which took place from the mid-2000s onwards, our dataset still contains over 5000 wells, which injected over 40 million m^3 of fluid.

Our HF-IS assessment results are shown in Fig. A.1. Only two events are potentially linked to HF wells – an M 2.9 event on 17/12/2015, and an M 2.0 event on 05/12/2020. Both of these events occur in areas where seismicity has previously been linked to WWD wells (Frohlich, 2012), and we believe that the links to HF wells identified are spurious, but we include them in our analysis for completeness.

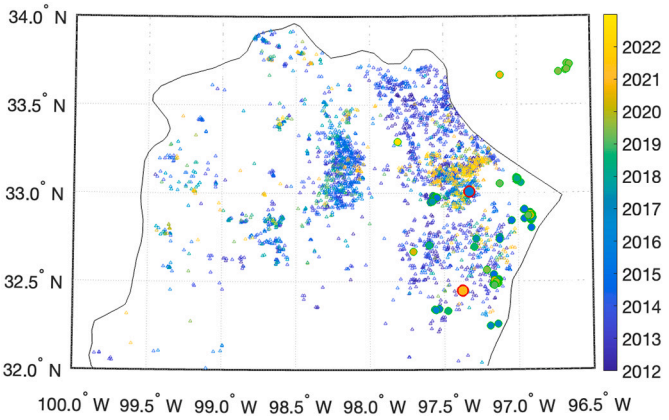

Fig. A.1. HF-IS assessment for the Barnett play. Triangles show HF wells, circles show earthquakes, coloured by date. Red-outlined earthquakes show cases linked to HF wells by our method. (For interpretation of the references to colour in this figure legend, the reader is referred to the web version of this article.)

A.1.2. Barnett Shale – Geological conditions

The Barnett Shale is of Mississippian age. It is underlain by the Ellenburger Formation. The Ellenburger is approximately 1 km thick, and has been a target for significant volumes of WWD. As such, any downward transfer of pressures from the Barnett would likely be absorbed within the Ellenburger and would not therefore be expected to engage basement structures. No high-resolution data from HF-IS cases has been recorded with which we might assess whether basement interactions have occurred. For the Barnett Shale pore pressures, McKeon (2011) specified $\Delta P_f = 0.52$ psi/ft., while Wang et al. (2013) specified a range from 0.45 to 0.52 psi/ft.

A.2. Eagle Ford Shale

The Eagle Ford play is located in southern Texas. This region has a long history of conventional oil and gas production. Unconventional production from the Eagle Ford Shale and the overlying Austin Chalk has developed from the late 2000s onwards. This play primarily produces shale oil rather than shale gas – while gas production has been moderate, oil production from the Eagle Ford represents the third-largest volume of any play in the US. Over 19,000 wells have been stimulated in the Eagle Ford and Austin Chalk.

Induced seismicity has been recognised in the Eagle Ford region since the 1970s, primarily associated with conventional production and WWD. Fasola et al. (2019) investigated a significant increase in seismicity that has taken place since 2014. They identified 94 M $\geq$ 2.0 earthquakes that were associated with HF. The largest event associated with HF reached M 4.0, making it the largest HF-induced event in the USA. Recent studies have provided details assessments of the relationships between HF-IS and mapped faults (McKeighan et al., 2022).

A.2.1. Eagle Ford induced seismicity assessment

We create a combined catalogue using the dataset published by Fasola et al. (2019), which runs from 2014 to 2018, to which we appended events from the TexNet catalogue from 2019 to the present. Well data in the FracFocus database for the Eagle Ford extends back to 2001, but significant numbers of wells are available from 2012 onwards. Given the available event catalogues, our analysis period runs from 2014 to the present. This time window contains over 15,000 wells, which cumulatively injected over 600 million m^3.

Over 380 events are linked to HF wells (Fig. A.2), a significant proportion of the overall number of recorded events. This is consistent with prior

studies (Fasola et al., 2019; McKeighan et al., 2022) that have concluded that the majority of seismicity in this play is now caused by hydraulic fracturing.

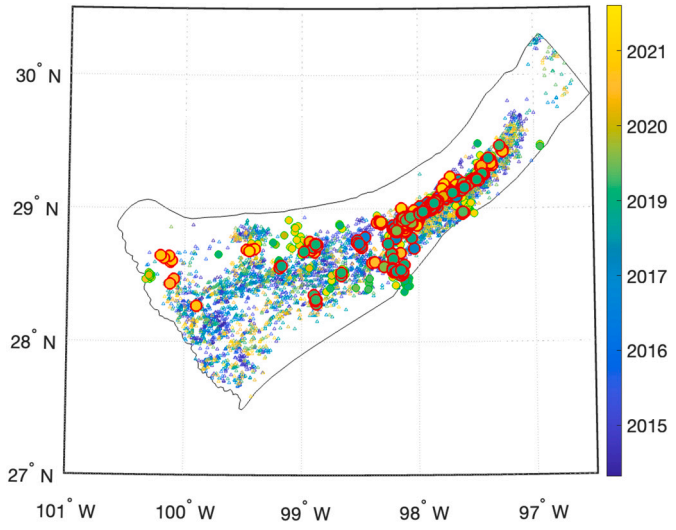

Fig. A1.2. HF-IS assessment for the Eagle Ford play.

A.2.2. Eagle Ford – Geological conditions

The Eagle Ford Shale is of Cenomanian (late-Cretaceous) age, and is underlain by a thick succession of lower Cretaceous and Jurassic sediments, most notably the Trinity Group. Locations of induced events in the Eagle Ford are provided by Li et al. (2021), although as the data are sourced from regional monitoring arrays, depth uncertainties are large. Li et al. (2021) located the majority of events below the Eagle Ford but within the underlying sedimentary strata (based on a comparison of event depths with crustal structure model of Cram, 1961). Hence, there is no evidence for engagement with basement strata for HF-IS in the Eagle Ford. For the Eagle Ford pore pressures, Wang et al. (2013) specified a range of ΔP_f from 0.5 to 0.8 psi/ft., while McKeon (2011) specified a range from 0.4 to 0.85 psi/ft.

A.3. Haynesville Shale

The Haynesville Shale straddles the border between Texas and Louisiana. It was one of the first shale plays to be developed after the Barnett, and it continues to be one of the most significant gas-producing plays in the USA. Over 5000 wells have been stimulated in the Haynesville and the overlying Bossier Formation. Only one case of HF-IS in the Haynesville has been reported, in Bienville Parish in 2011 (Walter et al., 2016), of which the largest event reached magnitude M 1.9. The Timpson earthquake sequence, which is linked to WWD (Frohlich et al., 2014) also occurred within this region.

A.3.1. Haynesville induced seismicity assessment

The FracFocus database contains large numbers of Haynesville wells from 2011 onwards. We compile a composite earthquake catalogue for the Haynesville by combining the data provided by Walter et al. (2016) with the TexNet catalogue. The Walter et al. (2016) catalogue extends between 2010 and 2012, while the TexNet catalogue runs from 2017, so our analysis is limited to between these two time windows. These time windows contain a total of over 3600 wells, which injected a total of over 200 million m^3, representing more than half of the total number of Haynesville wells in the FracFocus database. Hence, while our assessment does not cover the entire development period for the play, a significant proportion is examined. The Bienville Parish HF-IS (Walter, 2016) falls below our M 2.0 magnitude threshold. However, two additional cases of HF-IS were identified (Fig. A.3), including a sequence in late 2018 straddling Nacogdoches and San Augustine Counties in Texas, in which the largest event reached M 3.6, and a sequence in Caddo Parish, Louisiana in April 2021 that reached M 3.8. Manual analysis of these two cases suggests that they are plausibly caused by HF-IS.

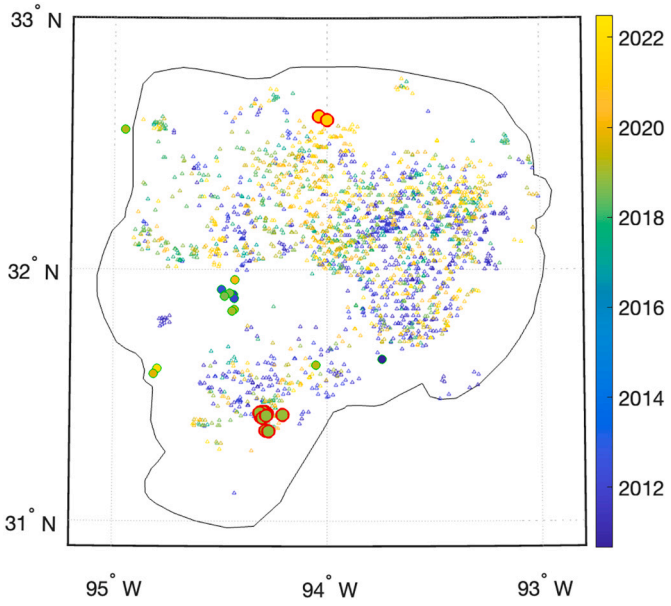

Fig. A.3. HF-IS assessment for the Haynesville play.

A.3.2. Haynesville – Geological conditions

The Haynesville Shale is of upper Jurassic age, and is found at depths of 3000–4000 m, in relatively close proximity to the basement. However, the lower Jurassic in the East Texas Basin includes the Louann Salt, which could present a hydraulic and geomechanical barrier to downward propagation of perturbations from the Haynesville. The earthquake depths from the only cases of induced seismicity within the Haynesville have large uncertainties, and so cannot constrain whether basement faults were involved. Pore pressures in the Haynesville are very overpressured. Wang et al. (2013) specified a range of ΔP_f from 0.7 to 0.95 psi/ft., while McKeon (2011) specified a range from 0.7 to 0.95 psi/ft.

A.4. Woodford Shale, Anadarko Basin, Oklahoma

The Woodford Shale is the primary target for unconventional gas development in the Anadarko Basin of Oklahoma. Several other formations, such as the underlying Viola Formation and the Mississippi Lime have also been targeted for unconventional development. Across Oklahoma, including the Arkoma Basin to the east, over 12,000 wells have been stimulated.

Oklahoma has seen one of the most significant increases in induced seismicity anywhere in the world, with the largest events exceeding M 5.0. Most of this seismicity has been generated by WWD into the deep-lying Arbuckle Formation (Keranen et al., 2013). However, detailed analysis by Skoumal et al. (2018) showed that there were a number of cases in the Anadarko Basin where seismicity was clearly associated with HF as well. In total, Skoumal et al. (2018) identified over 700 events with M $\geq$ 2.0 that were associated with 274 HF wells, with the largest event reaching M 3.5. In some areas, over 50% of wells were associated with induced seismicity.

A.4.1. Woodford induced seismicity assessment

We limit our analysis to the Woodford Shale play within the Anadarko Basin, where Skoumal et al. (2018) identified a significant proportion of HF-IS. Extending our analysis to other regions of Oklahoma may risk mischaracterisation of the significant quantities of WWD-induced seismicity.

The earliest entry in the FracFocus database for this area is from 2008, but entries for significant numbers of wells are found from 2011 onwards. We use earthquakes from the Oklahoma Geological Survey catalogue (Walter et al., 2020), which contains events from 1980 onwards, although significant numbers of events are catalogued from 2010 onwards. Our analysis runs from 2011 to the present, containing over 4400 wells which have injected a combined total of nearly 200 million m^3.

Of >1100 recorded events within the play, we link nearly 800 to HF wells (Fig. A.4), confirming the conclusions of Skoumal et al. (2018) that the majority of seismicity within this region of Oklahoma is in fact induced by HF rather than WWD. The largest HF-IS event reached M 3.6.

A.4.2. Woodford Shale – Geological conditions

The Woodford Formation in the Anadarko Basin is of upper Devonian age. The distance between the basement and target HF formations varies significantly in the Anadarko Basin, but across the basin the basement is overlain by the Arbuckle Formation, which has been the target for extensive WWD. We anticipate that downward transfer of pressure from the Woodford would be absorbed within the Arbuckle and so would not be transferred to the basement.

Ries et al. (2020) performed a detailed assessment of geological factors that correlated with HF-IS in the Anadarko Basin. They found that the prevalence of HF-IS increased with formation depth, but did not increase with proximity to basement (somewhat paradoxically, as formations move deeper into the basin, their distance from basement increases as the overall sediment column increases in thickness as well). This would imply that connections to basement are not a significant factor for HF-IS in the Woodford Formation. Nelson and Gianoutsos (2014) presented ΔP_f data for the Woodford Shale, with ΔP_f ranging from 0.5 to 0.9 psi/ft. McKeon et al. (2011) specified ΔP_f ranging from 0.45 to 0.68 psi/ft. for the Woodford.

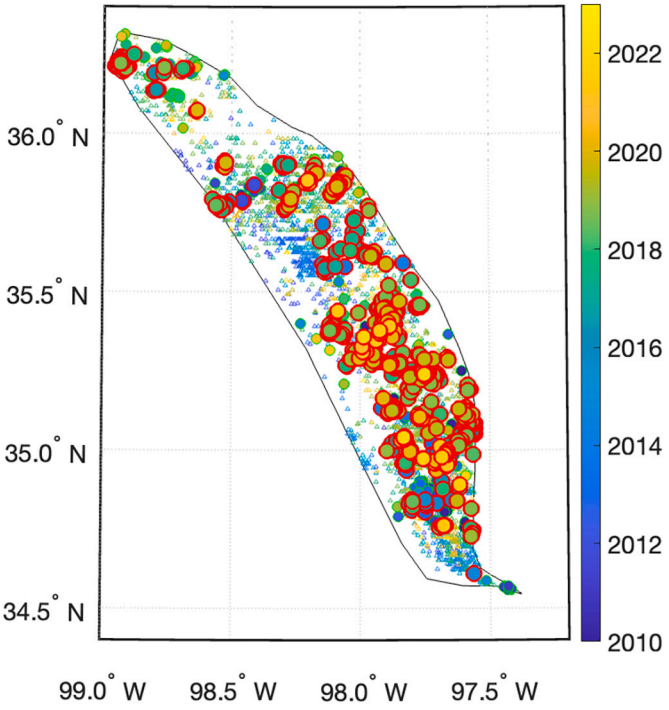

Fig. A.4. HF-IS assessment for the Woodford play within the Anadarko Basin of Oklahoma.

A.5. Fayetteville Shale

The Fayetteville Shale in Arkansas was one of the first shale gas plays to be developed after the Barnett Shale, though it has decreased in significance through the 2010s. There have been over 2500 HF wells completed in the Fayetteville. WWD also takes place into the underlying Ozark Formation.

From 2009, a sequence of seismicity was observed along a trend between the cities of Guy and Greenbrier (Horton, 2012), the largest of which reached M 4.7 in 2011. This seismicity was initially thought to be solely attributable to WWD in the Ozark Formation. However, re-appraisal of the sequence by Yoon et al. (2017) showed that a subset of events that were clearly linked to HF activities in the Fayetteville. Yoon et al. (2017) characterised 10 sub-clusters of events as being caused by HF, the largest of which reached M 2.9.

A.5.1. Fayetteville induced seismicity assessment

We use the Arkansas earthquake catalogue from the Arkansas Geological Survey for our analysis, which runs until 2021, with a significant increase in events occurring from 2010 onwards. The FracFocus database contains significant numbers of well entries from 2010 onwards. Our analysis therefore runs from 2010 to the present, which includes with over 2800 wells, injecting a cumulative total of over 27 million m^3.

We find over 300 events that could be linked to HF wells within the play. A subset of these events (approximately 100) were found within the Guy-Greenbrier lineament and so may represent WWD-induced cases (discriminating between causal factors in this area is challenging, as discussed by Yoon et al., 2017). However, outside of the Guy-Greenbrier lineament, over 200 presumed HF-IS events were also identified, including the largest magnitude case, an M 3.8 event on 04/06/2014 in eastern Van Buren County. These examples confirm the conclusions reached by Yoon et al. (2017), that in addition to WWD induced seismicity along the Guy-Greenbrier trend, significant numbers of events have been caused by hydraulic fracturing elsewhere in the play.

A.5.2. Fayetteville – Geological conditions

The Fayetteville Shale is of Mississippian age. In the region of the Fayetteville that experienced HF-IS, stimulation depths are typically around 2 km (Yoon et al., 2017). The Fayetteville is separated from the Precambrian basement by approximately 2 km of sediments (Ogwari et al., 2016), including the Ozark Formation, which was the target for the WWD that has triggered the bulk of the induced seismicity in the area. However, faults do extend from the basement upwards into the Carboniferous (Ogwari et al., 2016). Depth locations for the Guy-Greenbrier induced seismicity are not well constrained. The WWD seismicity occurs within the Ozark and within the underlying basement. However, the locations from Yoon et al. (2017) appear to show that the clusters associated with HF are located above the basement. We were not able to identify any data pertaining to pore pressure in the Fayetteville, and so for the purposes of our analysis adopt the same values as the Woodford as the nearest analogue play.

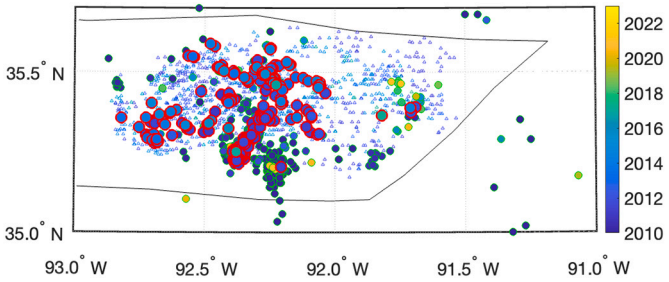

Fig. A.5. HF-IS assessment for the Fayetteville Shale.

A.6. Marcellus Shale

The Marcellus Shale is found in the Appalachian Basin, running through Virginia, Ohio, New York, and Pennsylvania. The bulk of production from the Marcellus occurs in Pennsylvania. Over 10,000 HF wells have been completed in the Marcellus. From 2013 until the present, the Marcellus has been the most productive shale play of any in the USA in terms of dry gas. A single case of HF-IS, located in Gilmer County, West Virginia, has been reported from stimulation of the Marcellus (Brudzinski and Kozłowska, 2019), with the largest event reaching M 2.7.

A.6.1. Marcellus induced seismicity assessment

For this region, the only catalogue available to us is the USGS Comprehensive Catalogue (ComCat). This data is of lower resolution in comparison to regional or local datasets analysed for other plays. The FracFocus database contains significant numbers of entries from 2011 onwards, with over 11,500 wells injecting a cumulative volume of over 450 million m^3.

Our analysis found two events linked to HF wells - this is the same July 2013 Gilmer County, West Virginia case identified by Brudzinski and Kozłowska (2019).

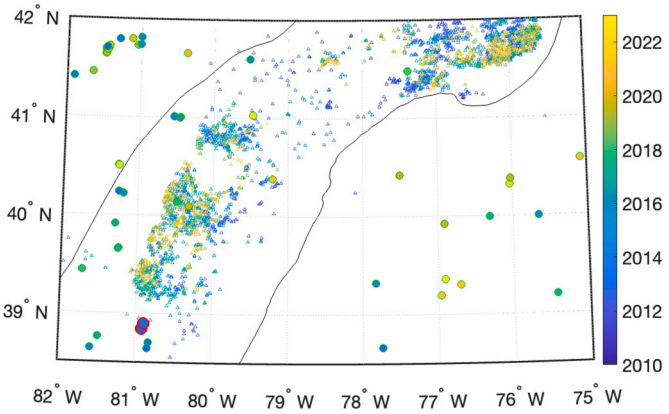

Fig. A.6. HF-IS assessment for the Marcellus Shale.

A.6.2. Marcellus Shale – Geological conditions

The Marcellus Shale is of Devonian age. Hydraulic fracturing in the Marcellus is usually situated more the 2 km above the basement. Skoumal et al. (2018b) identified that the Salinas evaporites, which underly the Marcellus, would provide a hydraulic and geomechanical barrier to any interaction with basement rocks. Only one case of induced seismicity has been recorded in the Marcellus, depth locations are not sufficiently precise to establish whether basement faults were involved. For the Marcellus, Wang et al. (2013) specified a range of ΔP_f from 0.44 to 0.7 psi/ft., while McKeon (2011) specified a range from 0.4 to 0.7 psi/ft.

A.7. Utica Shale

The Utica Shale is also found in the Appalachian Basin, underlying the Marcellus: the Marcellus is of middle-Devonian age, whereas the Utica is upper-Ordovician. Production from the Utica has generally been focussed further eastwards in Ohio. Total gas production from the Utica has been approximately 20% of that from the overlying Marcellus, and over 3000 wells have been drilled. In addition to HF in the Utica, WWD in Ohio is conducted into the underlying Mt. Simon formation.

Kozłowska et al. (2018) identified at least 5 sequences of HF-IS in Harrison County, Ohio, that occurred between 2013 and 2015. Brudzinski and Kozłowska (2019) identified further HF-IS sequences in Mahoning, Belmont, Noble and Monroe Counties continuing until at least 2017. They estimated that approximately 50 HF wells in Ohio had experienced some induced seismicity. The largest event associated with HF reached M 3.7.

A.7.1. Utica induced seismicity assessment

For this region, the only catalogue available to us is the USGS ComCat. This data is of lower resolution in comparison to regional or local datasets analysed for other plays. The FracFocus database contains significant numbers of entries from 2011 onwards, with over 3000 wells injecting a

cumulative volume of over 150 million m^3.

We identified 8 events linked to HF wells in 5 clusters (Fig. A.7). These cases included the June 2017 Noble County case, which contained the largest event of M 3.4. In addition to the cases identified by Brudzinski and Kozłowska (2019), we identify a sequence in October/November 2021 in Carroll County.

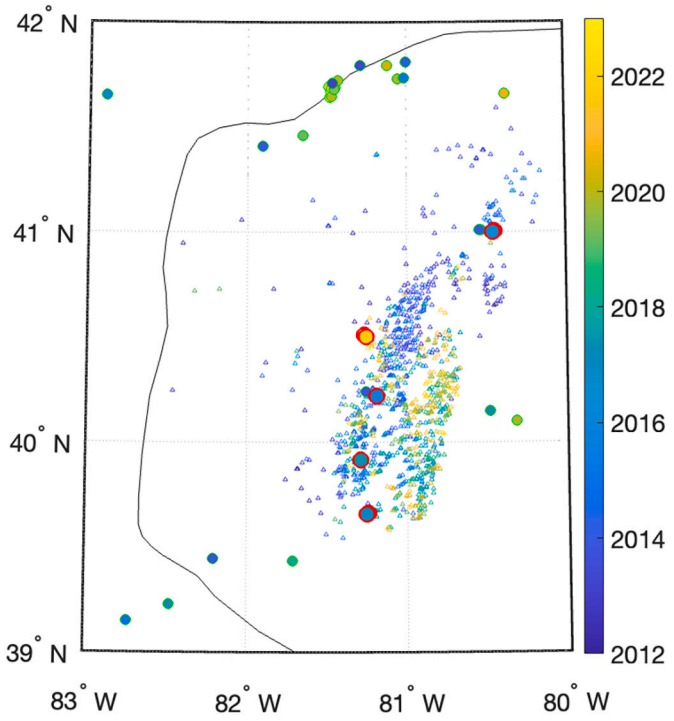

Fig. A.7. HF-IS assessment for the Utica Shale.

Brudzinski and Kozłowska (2019) developed a higher resolution catalogue for Ohio using local stations and template matching. They identified at least 35 M $\geq$ 2.0 events associated with hydraulic fracturing. While there is overlap between the events identified here and the Brudzinski and Kozłowska (2019) study, it is clear that their catalogues have identified a larger number of HF-IS cases. Hence, in our assessment in Table 2, our analysis is based on the numbers and magnitudes of events detected by Brudzinski and Kozłowska (2019), with the addition of the 2021 Carroll County events.

A.7.2. Utica Shale – Geological conditions

The Utica Shale is of Ordovician age and is typically >1 km below the Marcellus, within 1 km of the basement. Kozłowska et al. (2018) provided high-resolution earthquake depths that show HF-IS from the Utica Shale extending downwards through underlying sediments, with the largest events occurring within the basement. Trotter (2018) provided a map of ΔP_f in the Utica. In east-central Ohio, where the induced seismicity has taken place, pore pressure gradients were in the range 12–16 ppg (0.62–0.83 psi/ft). WVU (2015) also mapped ΔP_f, with values of 0.7–0.9 psi/ft. in east-central Ohio.

A.8. Niobrara Shale

The Niobrara Formation is situated in the Denver-Julesburg and Powder River Basins, primarily in Colorado and extending into Wyoming and Nebraska. It is primarily an oil play, with relatively moderate gas production. Though it is a carbonate formation, hydraulic fracturing is extensively used to generate commercial production, both in the Niobrara and in the underlying Pierre Shale. Conventional production from the Niobrara has taken place since the 1970s, but decreased through the early 2000s, before experiencing a renaissance with the use of hydraulic fracturing (Han et al., 2019).

Induced seismicity in the Denver Basin has been generated by WWD at the Rocky Mountain Arsenal (e.g., Healy et al., 1968) and at Greeley (Yeck et al., 2016), and WWD-induced seismicity has also been observed in the Raton Basin to the south. However, no induced seismicity has been reported from hydraulic fracturing in the Niobrara Formation.

A.8.1. Niobrara induced seismicity assessment

For this region, we append the catalogue developed by Yeck et al. (2016) for the Greeley WWD-induced seismicity to data from the USGS ComCat. The Yeck et al. (2016) catalogue runs from 2014 to 2021, but only covers a small area within the Niobrara play. The ComCat catalogue has broad spatial and temporal coverage, but at limited resolution. The FracFocus database has significant numbers of entries for Niobrara wells from 2011 onwards. Our analysis window runs from 2011 to the present and includes over 17,000 wells which injected a total of over 360 million m^3.

Nine events are linked to HF wells by our analysis, however all of these events are within the Greeley cluster identified by Yeck et al. (2016), and so the identified links with HF are likely to be spurious, but we include them in our analysis for completeness.

A.8.2. Niobrara – Geological conditions

The Niobrara Formation is of Upper Cretaceous age, at depths of 1.5–2.5 km, approximately 1 km above the basement. The underlying formations include a significant thickness of Permian salt deposits which could provide a barrier to downward propagation of pressure or stress perturbations. No cases of HF-IS have been reported from the Niobrara with which we might assess whether basement interactions have occurred. Sonnenberg (2015) reports ΔP_f values for the Niobrara of between 0.5 and 0.65 psi/ft.

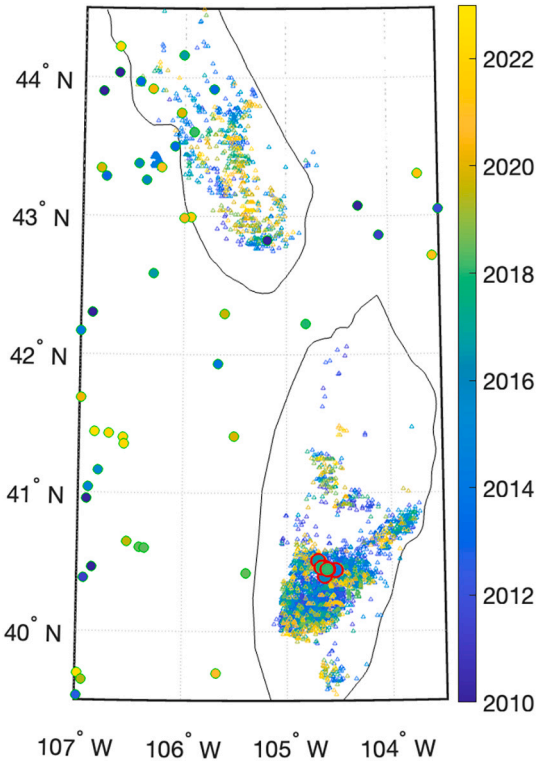

Fig. A.8. HF-IS assessment for the Niobrara Shale.

A.9. Bakken Shale

The Bakken Shale is found in the Williston Basin, in North Dakota, Montana, and into Saskatchewan, Canada. It is primarily a shale oil play, so while gas volumes are small, the play is the second-largest oil producer in the USA (after the Permian Basin). Over 15,000 wells have been drilled in North Dakota targeting the Bakken, with over 2000 wells in Saskatchewan. In addition, significant volumes of wastewater are injected into shallower Cretaceous aquifers (Verdon et al., 2016). Induced seismicity has been observed in the Williston Basin associated with potash dissolution mining (Verdon et al., 2016). However, no induced seismicity has been reported associated with either WWD or HF.

A.9.1. Bakken induced seismicity assessment

We use the catalogue compiled by Verdon et al. (2016) using USArray stations and local temporary stations deployed at the Weyburn and Aquistore CCS sites, to which we append events from the USGS ComCat. The FracFocus database has significant numbers of entries for Bakken wells from 2011 onwards. Our analysis window runs from 2011 to the present and includes over 15,000 wells which injected a total of over 280 million m^3.

A single M 3.3 event on 28/09/2012 is associated with an HF well. Given the numbers of wells stimulated, and the fact that this is a single isolated event, this link is likely to be coincidental. However, we include this in our analysis for completeness. Our analysis only covers the portion of the Bakken within the United States. However, Verdon et al. (2016) have previously examined whether HF-IS had occurred in the Canadian portion of the Bakken play, and did not find any candidate events.

A.9.2. Bakken – Geological conditions

The Bakken Formation is of late-Devonian/early-Carboniferous age, at depths of approximately 2–3 km. The Bakken is underlain by significant thicknesses of lower Devonian and Cambrian strata. Hydraulic fracturing is generally at least 1–2 km above the basement, with salts of the Prairie Formation acting as a potential geomechanical and hydraulic barrier. McKeon (2011) gives a range of ΔP_f for the Bakken of 0.5–0.6 psi/ft. Ganpule et al. (2015) provide a map of estimated ΔP_f values across the play, with values across the prospective areas of the play ranging from 0.68 to 0.78 psi/ft.

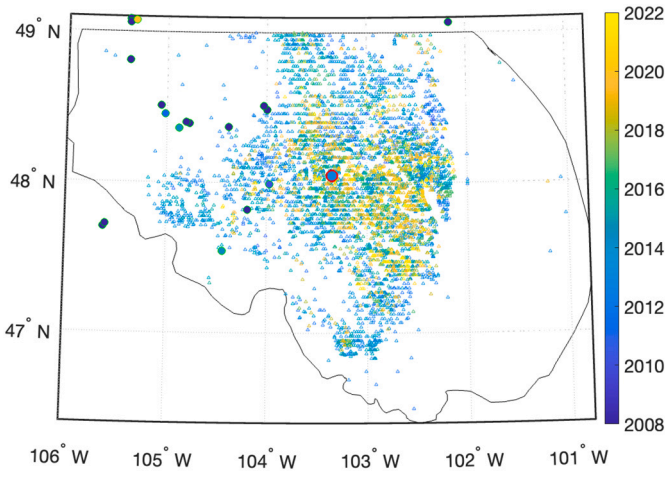

Fig. A.9. HF-IS assessment for the Bakken Shale.

A.10. Duvernay Shale

The Duvernay Shale is found in the WCSB, covering approximately 20% of the area of Alberta. The WCSB has seen extensive hydrocarbon development, including the use of hydraulic fracturing in shallower, tight gas formations such as the Cardium and Mannville. Development of the Duvernay Shale with hydraulic fracturing began in the early 2010s, and development has focussed on two areas – Fox Creek in northwest Alberta, and Willisden Green in central Alberta. Nearly 2000 wells have been stimulated in the Duvernay Formation. Extensive WWD also takes place across the WCSB, targeting formations at a range of depths.

The Duvernay Shale has been one of the most prolific of any play in terms of HF-IS, and HF-IS in the Duvernay is perhaps the most widely studied. There have been over 40 M $\geq$ 3.0 events associated with HF in the Duvernay, with 3 exceeding M 4.0 and the largest reaching M 4.2. Initially, HF-IS was confined to the Fox Creek region (Schultz et al., 2017), but later developments near to the city Red Deer have also produced HF-IS (Schultz and Wang, 2020).

A.10.1. Duvernay Shale induced seismicity assessment

We use the Composite Alberta Seismicity Catalogue (CASC, Fereidoni and Cui, 2015) for our assessment. We use the well database compiled by the Alberta Energy Regulator, using records available from 2000 onwards. A significant increase in hydraulic fracturing is found from 2010 onwards, but since we believe the dataset to be relatively complete, we include the period from 2000 onwards in our study. This period includes over 1900 wells, which injected a cumulative volume of over 44 million m^3.

We find over 500 events associated with Duvernay wells. The associated events are primarily found in two clusters around Fox Creek to the northwest, and Willisden Green to the southeast, as identified respectively by Schultz et al. (2017) and Schultz and Wang (2020). A single case is identified within the Rocky Mountain House cluster, which is known to be driven by gas production in the Strachan Field (Wetmiller, 1986) – the association made in our study likely to be a false positive.

A.10.2. Duvernay Shale – Geological conditions

The Devonian-age Duvernay Shale is perhaps the most extensively studied of any shale play in terms of induced seismicity. High resolution microseismic monitoring has revealed in detail the interactions between hydraulic fractures and pre-existing faults that have generated induced seismicity (e.g., Igonin et al., 2021, 2022). The Duvernay is found within a few hundred meters of the basement, separated only by the carbonates of the Beaverhill Lake Group. Microseismic monitoring has revealed induced seismicity occurring on faults that extend upwards from the basement (e.g., Eaton et al., 2018; Eyre et al., 2019), and in some cases, the induced seismicity has been located within the basement (e.g., Bao and Eaton, 2016). Eaton and Schultz (2018) mapped pore pressure gradients across the Duvernay. They found a range of ΔP_f from 11 to 20 kPa/m, but identified that seismicity only occurs where pressures exceed 15 kPa/m, and the bulk of the seismicity is found where $\Delta P_f \approx 20$ kPa/m.

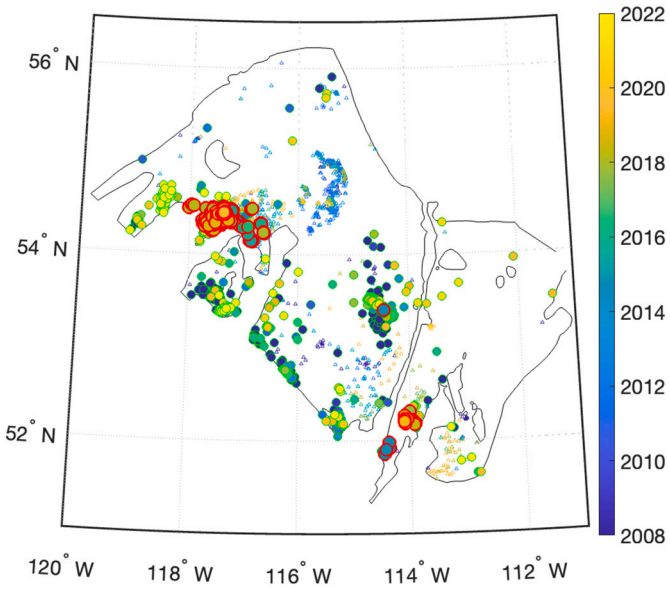

Fig. A.10. HF-IS assessment for the Duvernay Shale.

A.11. Montney Shale

The Montney Formation in the WCSB runs from northwest Alberta into B.C., in some places overlying the deeper Duvernay Formation. Unlike the Duvernay, much of the production from the Montney takes place within the fold-and-thrust belt associated with the Laramide orogeny. Initially, the Montney hosted small volumes of conventional production from sandstone layers within the formation. From the mid 2000s onwards, hydraulic fracturing has been used to develop the shale.

Much like the Duvernay, the Montney has been one of the most prolific, and most widely studied play in terms of HF-IS. Over 40 M $\geq$ 3.0 events have been associated with HF in the Montney, with 4 exceeding M 4.0 and largest being M 4.6. The HF-IS in the Montney has occurred in two regions (BCOGC, 2014): within the Rocky Mountain fold-and-thrust belt, and within the Peace River arch, a zone around Fort St John with cratonic uplift and an increased abundance of Palaeozoic normal faulting (Mossop and Shetsen, 1994).

A.11.1. Montney induced seismicity assessment

We use the CASC earthquake catalogue for our assessment, and well data compiled from the AER and the B.C. Oil and Gas Commission, using data from 2000 onwards. We limit our analysis to a region north of 55° latitude – south of this area there is overlap between the Montney and Duvernay plays, and detailed seismological analysis has shown that the seismicity in this region (namely, the Fox Creek region) is caused exclusively by hydraulic fracturing in the Duvernay (Schultz et al., 2015). This region includes over 8000 Montney wells, which have injected nearly 80 million m^3.

Nearly 400 events are linked to Montney wells. The majority of these are within the Rocky Mountain fold-and-thrust belt and the Peace River arch, as identified by previous studies (e.g., BCOGC, 2014).

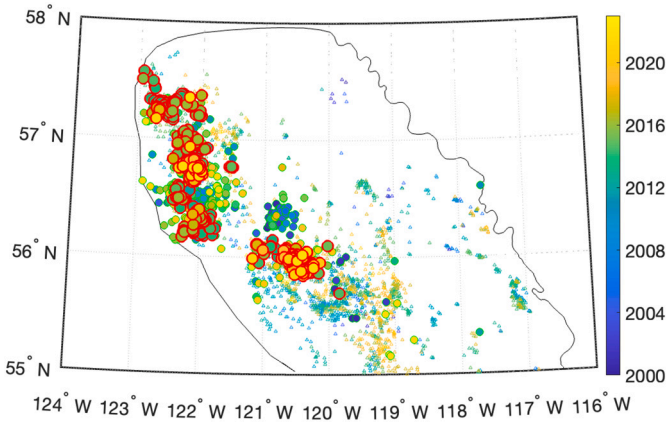

Fig. A.11. HF-IS assessment for the Montney Shale.

A.11.2. Montney – Geological conditions

The Triassic-age Montney Shale has also been extensively studied with detailed microseismic observations of HF-IS (e.g., Riazi and Eaton, 2020). The Montney is found at depths of around 2 km, with a thick succession of underlying Carboniferous and Devonian sediments between the formation and basement rocks. Detailed microseismic observations from Riazi and Eaton (2020) show induced seismicity within the Montney occurring on thrust

faults associated with the Rocky Mountain fold-and-thrust belt. These faults can be mapped in 3D reflection data and are shown to sole out in Devonian strata, and do not connect to the basement. Eaton and Schultz (2018) mapped pore pressure gradients across the Duvernay. They found a range of ΔP_f from 11 to 20 kPa/m, but identified that seismicity only occurs where pressures exceed 15 kPa/m, and the bulk of the seismicity is found where $\Delta P_f \approx$ 20 kPa/m.

A.12. Horn River Shale

The Horn River Shale is situated in northeastern B.C.. The shale is often divided into three members, the Evie, Muskwa and Otter Park, but we group these as a single unit here. Over 500 wells have been stimulated in this play, with production increasing significantly from 2008. From the mid-2010s, development in this play has diminished significantly because of a lack of commercial viability. HF-IS was first observed in the Horn River play in 2008 (BCOGC, 2012), making this the first recorded example of induced seismicity from shale gas development anywhere in the world (Farahbod et al., 2015). >20 M $\geq$ 3.0 induced events have since been identified, with the largest reaching M 3.6.

A.12.1. Horn River induced seismicity assessment

We use the CASC earthquake catalogue for our assessment. We use well data from the BCOGC database, the majority of which date from between 2008 and 2014. This database contains approximately 350 wells, which injected a total of 14 million m^3.

Most of the 42 recorded earthquakes within the play are associated with Horn River wells, with cases running from 2009 to 2012, and a largest event magnitude of M 3.6.

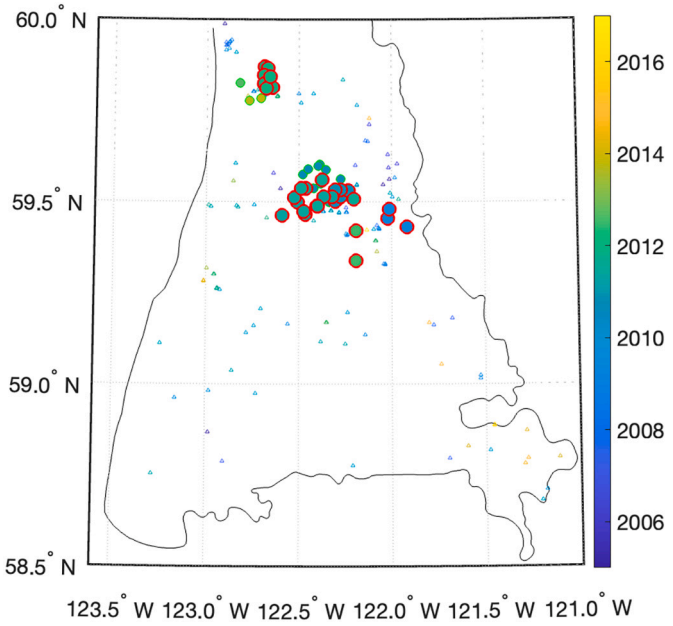

Fig. A.12. HF-IS assessment for the Horn River Shale.

A.12.2. Horn River – Geological conditions

The Horn River Shale is of Devonian age, and is found at depths of about 2–3 km. We were not able to identify any detailed data regarding the depths from the Horn River to the basement, but based on structure contours from Mossop and Shetsen (1994), it is likely to be within a few hundred m. The BCOGC (2012) report identified faults extending from the basement into the Devonian section. By analogy with HF-IS in the Devonian-age Duvernay Formation, it is reasonable to believe that these basement-seated faults are responsible for the HF-IS in the Horn River Formation. Reynolds and Munn (2010) report a pore pressure gradient for the Horn River of 0.75 psi/ft., while Latimer et al. (2017) give a range from 11 to 18 kPa/m.

References from Appendix.

Bao X. and D.W. Eaton, 2016. Fault activation by hydraulic fracturing in Western Canada: Science 354, 1406–1409.

BCOGC, 2012. Investigation of observed seismicity in the Horn River Basin. B.C. Oil and Gas Commission: Available online at https://www.bcogc.ca/node/8046/download.

BCOGC, 2014. Investigation of observed seismicity in the Montney Trend. B.C. Oil and Gas Commission: Available online at https://www.bcogc.ca/node/12291/download.

Brudzinski, M.R., and M. Kozłowska, 2019. Seismicity induced by hydraulic fracturing and wastewater disposal in the Appalachian Basin, USA: a review: Acta Geophysica 67, 351–364.

Cram, I.H., 1961. A crustal structure refraction survey in south Texas: Geophysics 26, 560–573.

Eaton, D.W., N. Igonin, A. Poulin, R. Weir, H. Zhang, S. Pellegrino, G. Rodriguez, 2018. Induced seismicity characterization during hydraulic-fracture monitoring with a shallow-wellbore geophone array and broadband sensors: Seismological Research Letters 89, 1641–1651.

Farahbod, A.M., H. Kao, D.M. Walker, J.F. Cassidy, 2015. Investigation of regional seismicity before and after hydraulic fracturing in the Horn River Basin, northeast British Columbia: Canadian Journal of Earth Sciences 52: 112–122.

Frohlich, C., 2012. Two year survey comparing earthquake activity and injection-well locations in the Barnett Shale: Proceedings of the National Academy of Science 109, 13,934–13,938.

Frohlich, C., W. Ellsworth, W.A. Brown, M. Brunt, J. Luetgert, T. MacDonald, S. Walter, 2014. The 17 May 2012 M 4.8 earthquake near Timpson, East Texas: An event possibly triggered by fluid injection: Journal of Geophysical Research 119, 581–593.

Ganpule, S., K. Srinivasan, T.M. Izykowski, B.A. Luneau, 2015. Impact of geomechanics on well completion and asset development in the Bakken formation: SPE Hydraulic Fracturing Technology Conference, The Woodlands, Texas, SPE 173329.

Han, Y., B. Horsfield, H. LaReau, N. Mahlstedt, 2019. Intraformational migration of petroleum: Insights into the development of sweet spot in the Cretaceous Niobrara shale-oil system, Denver Basin: Marine and Petroleum Geology 107, 301–309.

Horton, S., 2012. Injection into subsurface aquifers triggers earthquake swarm in central Arkansas with potential for damaging earthquake: Seismological Research Letters 83, 250–260.

Latimer, A., M. Hill, J. Hendrick, 2017. Pore pressure anomalies in the Horn River Basin, northeastern BC: Geoconvention Conference, Calgary.

Mossop, G.D. and I. Shetsen, 1994. Geological atlas of the Western Canada Sedimentary Basin: Canadian Society of Petroleum Geologists and Alberta Research Council. Available at https://ags.aer.ca/reports/atlas-of-the-western-canada-sedimentary-basin.htm.

Nelson, P.H., and N.J. Gianoutsos, 2014. Potentiometric surfaces for seven stratigraphic units and an explanation for underpressure in the Greater Anadarko Basin, Oklahoma, Texas, Kansas, and Colorado: in D.K. Higley, ed., Petroleum systems and assessment of undiscovered oil and gas in the Anadarko Basin Province, Colorado, Kansas, Oklahoma, and Texas - USGS Province 58: U.S. Geological Survey Digital Data Series.

Ogwari, P.O., S.P. Horton, S. Ausbrooks, 2016. Characteristics of induced/ triggered earthquakes during the startup phase of the Guy-Greenbrier earthquake sequence in north-central Arkansas: Seismological Research Letters 87, 620–630.

Quinones, L., H.R. DeShon, S. Jeong, P. Ogwari, O. Sufri, M.M. Holt, K.B. Kwong, 2019. Tracking induced seismicity in the Fort Worth basin: a summary of the 2008–2018 North Texas earthquake study catalogue: Bulletin of the Seismological Society of America 109, 1203–1216.

Reynolds, M.M. and D.L. Munn, 2010. Development update for an emerging shale gas giant field - Horn River Basin, British Columbia, Canada: SPE Unconventional Gas Conference, Pittsburgh, SPE-130103.

Riazi, N., and D. Eaton, 2020. Anatomy of a buried thrust belt activated during hydraulic fracturing: Tectonophysics 795, 228,640.

Skoumal, R.J, M.R. Brudzinski, B.S. Currie, 2018b. Proximity of Precambrian basement affects the likelihood of induced seismicity in the Appalachian, Illinois, and Williston Basins, central and eastern United States: Geosphere 14, 1365–1379.

Sonnenberg, S.A., 2015. New reserves in an old field, the Niobrara/Codell resource plays in the Wattenberg Field, Denver Basin, Colorado: First Break 33, 55–62.

Trotter, B., 2018. Pore pressure prediction in the Point Pleasant formation in the Appalachian Basin, in parts of Ohio, Pennsylvania, and West Virginia, United States of America: PhD Thesis, Ohio State University.

Verdon, J.P., J-M. Kendall, A.C. Horleston, A.L. Stork, 2016. Subsurface fluid injection and induced seismicity in southeast Saskatchewan: International Journal of Greenhouse Gas Control 54, 429–440.

Walter, J.I., P.J. Dotray, C. Frohlich, J.F.W. Gale, 2016. Earthquakes in northwest Louisiana and the Texas–Louisiana border possibly induced by energy resource activities within the Haynesville Shale play: Seismological Research Letters 87, 285–294.

Wang, F.P., U. Hammes, R. Reed, T. Zhang, X. Tang, Q. Li, 2013. Petrophysical and mechanical properties of organic-rich shales and their influences on fluid flow: in J. Chatellier and D. Jarvie, eds., Critical assessment of shale resource plays: AAPG Memoir 103, 167–186.

Wetmiller, R.J., 1986. Earthquakes near Rocky Mountain House, Alberta, and their relationship to gas production facilities: Canadian Journal of Earth Sciences 23, 172–181.

WVU, 2015. A geologic play book for Utica Shale Appalachian Basin exploration: Utica Shale Appalachian Basin Exploration Consortium, West Virginia University.

References

Cao, W., Verdon, J.P., Tao, M., 2022. Coupled poroelastic modelling of hydraulic fracturing-induced seismicity: Implications for understanding the post shut-in M_L 2.9 earthquake at the Preston New Road, UK. J. Geophys. Res. 127 e2021JB023376.

Clarke, H., Eisner, L., Styles, P., Turner, P., 2014. Felt seismicity associated with shale gas hydraulic fracturing: the first documented example in Europe. Geophys. Res. Lett. 41, 8308–8314.

Clarke, H., Verdon, J.P., Kettlety, T., Baird, A.F., Kendall, J.-M., 2019. Real time imaging, forecasting and management of human-induced seismicity at Preston New Road, Lancashire, England. Seismol. Res. Lett. 90, 1902–1915.

Deng, K., Liu, Y., Harrington, R.M., 2016. Poroelastic stress triggering of the December 2013 Crooked Lake, Alberta, induced seismicity sequence. Geophys. Res. Lett. 43, 8482–8491.

Dinske, C., Shapiro, S.A., 2013. Seismotectonic state of reservoirs inferred from magnitude distributions of fluid-induced seismicity. J. Seismol. 17, 13–25.

Dundon, L.A., Abkowitz, M., Camp, J., 2015. The real value of FracFocus as a regulatory tool: a national survey of state regulators. Energy Policy 87, 496–504.

Eaton, D.W., Schultz, R., 2018. Increased likelihood of induced seismicity in highly overpressured shale formations. Geophys. J. Int. 214, 751–757.

Fasola, S.L., Brudzinski, M.R., Skoumal, R.J., Langenkamp, T., Currie, B.S., Smart, K.J., 2019. Hydraulic fracture injection strategy influences the probability of earthquakes in the Eagle Ford Shale play of South Texas. Geophys. Res. Lett. 46, 12958–12967.

Fereidoni, A., Cui, L., 2015. Composite Alberta Seismicity Catalog: CASC2014-x. Available at: https://www.inducedseismicity.ca/wp-content/uploads/2015/01/Composite-Alberta-Seismicity-Catalog3.pdf.

Fox, A., McKean, S., Watson, N., 2020. Statistical assessment of operational risks for induced seismicity from hydraulic fracturing in the Montney, Northeast BC. Geosci. BC Rep. 2020–12. Available at: https://cdn.geosciencebc.com/project_data/GBCReport2020-12/Geoscience%20BC%20Report%202020-12%20FINAL%20REPORT.pdf last accessed on 15/05/2023.

Galloway, E., Hauck, T., Corlett, H., Pană, D., Schultz, R., 2018. Faults and associated karst collapse suggest conduits for fluid flow that influence hydraulic fracturing-induced seismicity. Proc. Natl. Acad. Sci. 115, E10003–E10012.

Gan, W., Frohlich, C., 2012. Gas injection may have triggered earthquakes in the Cogdell oil field, Texas. Proc. Natl. Acad. Sci. 110, 18786–18791.

Ghofrani, H., Atkinson, G.M., 2020. Activation rate of seismicity for hydraulic fracture wells in the Western Canada Sedimentary Basin. Bull. Seismol. Soc. Am. 110, 2252–2271.

Grigoratos, I., Rathje, E., Bazzurro, P., Savvaidis, A., 2020. Earthquakes induced by wastewater injection, part I: model development and hindcasting. Bull. Seismol. Soc. Am. 110, 2466–2482.

Gutenberg, B., Richter, C.F., 1944. Frequency of earthquakes in California. Bull. Seismol. Soc. Am. 34, 185–188.

Hallo, M., Oprsal, I., Eisner, L., Ali, M.Y., 2014. Prediction of magnitude of the largest potentially induced seismic event. J. Seismol. 18, 421–431.

Healy, J.H., Rubey, W.W., Griggs, D.T., Raleigh, C.B., 1968. The Denver earthquakes. Science 161, 3848.

Hincks, T., Aspinall, W., Cooke, R., Gernon, T., 2018. Oklahoma's induced seismicity strongly linked to wastewater injection depth. Science 359, 1251–1255.

Igonin, N., Verdon, J.P., Kendall, J.-M., Eaton, D.W., 2021. Large-scale fracture systems are permeable pathways for fault activation during hydraulic fracturing. J. Geophys. Res. 126 e2020JB020311.

Igonin, N., Verdon, J.P., Eaton, D.W., 2022. Seismic anisotropy reveals stress changes around a fault as it is activated by hydraulic fracturing. Seismol. Res. Lett. 93, 1737–1752.

Keranen, K.M., Savage, H.M., Abers, G.A., Cochran, E.S., 2013. Potentially induced earthquakes in Oklahoma: USA: links between wastewater injection and the 2011 M_W 5.7 earthquake sequence. Geology 41, 699–702.

Kettlety, T., Verdon, J.P., Werner, M., Kendall, J.-M., 2020. Stress transfer from opening hydraulic fractures controls the distribution of induced seismicity. J. Geophys. Res. 125 e2019JB018794.

Kettlety, T., Verdon, J.P., Butcher, A., Hampson, M., Craddock, L., 2021. High-resolution imaging of the M_L 2.9 August 2019 earthquake in Lancashire, United Kingdom, induced by hydraulic fracturing during Preston New Road PNR-2 operations. Seismol. Res. Lett. 92, 151–169.

Kwiatek, G., Saamo, T., Ader, T., Bluemle, F., Bohnhoff, M., Chendorain, M., Dresen, G., Heikkinen, P., Kukkonen, I., Leary, P., Leonhardt, M., Malin, P., Martinez-Garzon, P., Passmore, K., Passmore, P., Valenzuela, S., Wollin, C., 2019. Controlling fluid-

induced seismicity during a 6.1-km-deep geothermal stimulation in Finland: Science. Advances 5 eaav7224.
Lund Snee, J.-E., Zoback, M.D., 2020. Multiscale variations of the crustal stress field throughout North America. Nat. Commun. 11, 1951.
McKeighan, C., Hennings, P., Horne, E.A., Smye, K., Morris, A., 2022. Understanding anthropogenic fault rupture in the Eagle Ford region, south-Central Texas. Bull. Seismol. Soc. Am. 112, 2870–2889.
McKeon, M., 2011. Horizontal Fracturing in Shale Plays: Halliburton.
Mustanen, D., Fianu, J., Pucknell, J., 2017. Account of hydraulically fractured onshore wells in the UK and seismicity associated with these wells. J. Pet. Sci. Eng. 158, 202–221.
NRC, 2013. Induced Seismicity Potential in Energy Technologies. The National Academies Press, Washington DC.
Pawley, S., Schultz, R., Playter, T., Corlett, H., Shipman, T., Lyster, S., Hauck, T., 2018. The geological susceptibility of induced earthquakes in the Duvernay Play. Geophys. Res. Lett. 45, 1786–1793.
Reyes-Canales, M., Rodriguez-Pradilla, G., Yusifbayov, J., van der Baan, M., 2022. The rise, peak and decline of the seismic hazard related to hydraulic fracturing activities in the Duvernay play, Fox Creek area, Alberta. J. Geophys. Res. 127 e2021JB023060.
Ries, R., Brudzinski, M.R., Skoumal, R.J., Currie, B.S., 2020. Factors influencing the probability of hydraulic fracturing-induced seismicity in Oklahoma. Bull. Seismol. Soc. Am. 110, 2272–2282.
Rodríguez-Pradilla, G., Eaton, D.W., Verdon, J.P., 2022. Basin-scale multi-decadal analysis of hydraulic fracturing and seismicity in western Canada shows non-recurrence of induced runaway fault rupture. Sci. Rep. 12, 14463.
Savvaidis, A., Young, B., Huang, G.D., Lomax, A., 2019. TexNet: a statewide seismological network in Texas. Seismol. Res. Lett. 90, 1702–1715.
Schultz, R., Wang, R., 2020. Newly emerging cases of hydraulic fracturing induced seismicity in the Duvernay East shale basin. Tectonophysics 779, 228393.
Schultz, R., Stern, V., Novakovic, M., Atkinson, G., Gu, Y.J., 2015a. Hydraulic fracturing and the Crooked Lake sequences: Insights gleaned from regional seismic networks. Geophys. Res. Lett. 42, 2750–2758.
Schultz, R., Skoumal, R.J., Brudzinski, M.R., Eaton, D., Baptie, B., Ellsworth, W., 2020. Hydraulic fracturing induced seismicity. Rev. Geophys. 58 e2019RG000695.
Schultz, R., Stern, V., Gu, Y.J., Eaton, D., 2015b. Detection threshold and location resolution of the Alberta Geological Survey earthquake catalogue. Seismol. Res. Lett. 86, 385–397.
Schultz, R., Corlett, H., Haug, K., Kocon, K., MacCormack, K., Stern, V., Shipman, T., 2016. Linking fossil reefs with earthquakes: geologic insight to where induced seismicity occurs in Alberta. Geophys. Res. Lett. 43, 2534–2542.
Schultz, R., Beroza, G.C., Ellsworth, W.L., 2021. A strategy for choosing red-light thresholds to manage hydraulic fracturing induced seismicity in North America. J. Geophys. Res. 126 e2021JB022340.
Segall, P., 1989. Earthquakes triggered by fluid extraction. Geology 17, 942–946.
Shapiro, S.A., Dinske, C., Langenbruch, C., 2010. Seismogenic index and magnitude probability of earthquakes induced during reservoir fluid stimulations. Lead. Edge 29, 304–309.
Simpson, R.W., 1997. Quantifying Anderson's fault types. J. Geophys. Res. 102, 17909–17919.
Skoumal, R.J., Ries, R., Brudzinski, M.R., Barbour, A.J., Currie, B.S., 2018. Earthquakes induced by hydraulic fracturing are pervasive in Oklahoma. J. Geophys. Res. 123, 10918–10935.
Stocker, M., Baffes, J., Vorisek, D., 2018. With the Benefit of Hindsight: The Impact of the 2014–16 Oil Price Collapse: In Global Economic Prospects, Broad Based Upturn, but for how Long? World Bank Group, Washington.
Verdon, J.P., Bommer, J.J., 2021a. Green, yellow, red, or out of the blue? An assessment of Traffic Light Schemes to mitigate the impact of hydraulic fracturing-induced seismicity. J. Seismol. 25, 301–326.
Verdon, J.P., Bommer, J.J., 2021b. Comment on "Activation rate of seismicity for hydraulic fracture wells in the Western Canadian Sedimentary Basin" by Ghofrani and Atkinson (2020). Bull. Seismol. Soc. Am. 111, 3459–3474.
Verdon, J.P., Baptie, B.J., Bommer, J.J., 2019. An improved framework for discriminating seismicity induced by industrial activities from natural earthquakes. Seismol. Res. Lett. 90, 1592–1611.
Walter, J.I., Ogwari, P., Thiel, A., Ferrer, F., Woelfel, I., Chang, J.C., Darold, A.P., Holland, A.A., 2020. The Oklahoma Geological Survey statewide seismic network. Seismol. Res. Lett. 91, 611–621.
Watkins, T.J.M., Verdon, J.P., Rodríguez-Pradilla, G., 2023. The temporal evolution of induced seismicity sequences generated by low-pressure, long-term fluid injection. J. Seismol. 27, 243–259.
Wozniakowska, P., Eaton, D.W., 2020. Machine learning-based analysis of geological susceptibility to induced seismicity in the Montney Formation, Canada. Geophys. Res. Lett. 47 e2020GL089651.
Zoback, M.D., Healy, J.H., 1992. In situ stress measurements to 3.5 km depth in the Cajon Pass Scientific Research Borehole: implications for the mechanics of crustal faulting. J. Geophys. Res. 97, 5039–5057.
Zoback, M.D., Townend, J., Grollimund, B., 2002. Steady-state failure equilibrium and deformation of intraplate lithosphere. Int. Geol. Rev. 44, 383–401.